Journal of Earth Science, *Vol. 28*, *No. 5*, *p. 897–916*, *October 2017* *ISSN 1674-487X*
Printed in China
https://doi.org/10.1007/s12583-017-0779-8

Organo-Petrographic and Pore Facets of Permian Shale Beds of Jharia Basin with Implications to Shale Gas Reservoir

Vinod Atmaram Mendhe*[1], Subhashree Mishra[1], Ranjit G. Khangar[3], Alka Damodhar Kamble[2], Durgesh Kumar[1], Atul Kumar Varma[4], H. Singh[1], Sujeet Kumar[1], Mollika Bannerjee[1]

1. *CSIR-Central Institute of Mining and Fuel Research*, *Dhanbad* 826 015, *India*
2. *IIT* (*ISM*)-*Department of Chemical Engineering*, *Indian Institute of Technology* (*ISM*), *Dhanbad* 826 004, *India*
3. *GSI-Geological Survey of India*, *Central Region*, *Nagpur* 440 006, *India*
4. *IIT* (*ISM*)-*Department of Applied Geology*, *Indian Institute of Technology* (*ISM*), *Dhanbad* 826 004, *India*

Vinod Atmaram Mendhe: http://orcid.org/0000-0003-3212-8298

ABSTRACT: The shale deposits of Damodar Valley have received great attention since preliminary studies indicate their potential for shale gas. However, fundamental information allied to shale gas reservoir characteristics are still rare in India, as exploration is in the primary stage. In this study, Barakar shale beds of eastern part of Jharia Basin are evaluated for gas reservoir characteristics. It is evident that Barakar shales are carbonaceous, silty, contains sub-angular flecks of quartz and mica, irregular hair-line fractures and showing lithological variations along the bedding planes, signifying terrestrial-fluviatile deposits under reducing environment. The values of TOC varies from 1.21 wt.% to 17.32 wt.%, indicating good source rock potentiality. The vitrinite, liptinite, inertinite and mineral matter ranging from 0.28 vol.% to 12.98 vol.%, 0.17 vol.% to 3.23 vol.%, 0.23 vol.% to 9.05 vol.%, and 74.74 vol.% to 99.10 vol.%, respectively. The ternary facies plot of maceral composition substantiated that Barakar shales are vitrinite rich and placed in the thermal-dry gas prone region. The low values of the surface area determined following different methods point towards low methane storage capacity, this is because of diagenesis and alterations of potash feldspar responsible for pore blocking effect. The pore size distribution signifying the micro to mesoporous nature, while Type II sorption curve with the H2 type of hysteresis pattern, specifies the heterogeneity in pore structure mainly combined-slit and bottle neck pores.

KEY WORDS: shale gas, petrographic composition, surface area, pore disposition, pore volume.

0 INTRODUCTION

In the recent years, shale gas has become very important to provide ample of hydrocarbon to balance the conventional resources deficit. Increased growth of natural gas production from shale gas reservoirs is due to the successful application and advances obtained in horizontal drilling and multi-stage hydraulic fracturing technologies (Shiver et al., 2015; Wang L et al., 2015; Loucks et al., 2009; Jarvie et al., 2007; Pollastro, 2007; Montgomery et al., 2005; Curtis, 2002). Shale gas is a natural gas (mostly methane) obtains from organically rich shales. Shales are fine grained, clastic sedimentary rock composed of mainly clay matters and tiny fragments of other minerals, especially quartz/mica and 2%–20% of organic matter (Varma et al., 2015; Hardy, 2014; Brown, 2009). Methane generated from the transformation of organic matter by bacterial action (biogenic gas) and geochemical (thermogenic gas) processes during the burial at variable depth (Passey et al., 2010; Claypool, 1998). Shales are the unconventional gas system where it acts as both source and reservoir rocks for gas mainly methane and is the store house of continuous petroleum accumulation (Jarvie et al., 2007; Schmoker, 1995). The process of adsorption plays an important role in unconventional resource for the retention of gas that is ultimately cracked to shale gas system (Jarvie, 2012). Organic matter in shale responsible for the in-situ gas generation which is stored in the micropore structure of organic matter (Loucks et al., 2009) and clay minerals (Varma et al., 2014; Ross and Marc, 2009; Chalmers and Bustin, 2007). The quality of shale reservoirs depends on their thickness and extent, organic content, thermal maturity, depth and pressure, fluid saturations and permeability (Mendhe et al., 2016, 2015a; Mishra et al., 2016; Ruppel et al., 2008). In India, shale gas can emerge as an important new source of energy. The shale gas formations are spread over in 26 sedimentary basins some of them are Jharia, Raniganj, Bokaro, Cambay, Gondwana, Krishna-Godavari and Cauvery containing thick shale beds of both Gondwana and Tertiary Period (Padhy and Das, 2013). Estimates of shale gas resources

*Corresponding author: vamendhe@gmail.com

Manuscript received April 11, 2017.
Manuscript accepted June 24, 2017.

Mendhe, V. A., Mishra, S., Khangar, R. G., et al., 2017. Organo-Petrographic and Pore Facets of Permian Shale Beds of Jharia Basin with Implications to Shale Gas Reservoir. *Journal of Earth Science*, 28(5): 897–916. https://doi.org/10.1007/s12583-017-0779-8. http://en.earth-science.net

in India vary from 63 trillion cubic feet (TCF) by Energy Information Administration and International Energy Agency (EIA, 2012, 2011; IEA, 2007) to as high as 2 000 TCF by Schlumberger (2012), of which the recoverable resources range between 100 and 300 TCF.

In this paper, through investigation of shales of Barakar Formation in Jharia Basin, India is presented. The results of analyses like technological properties, rockeval and TOC, maceral-mineral composition, vitrinite reflectance and low pressure N_2 sorption isotherm are relatively correlated. The depositional process of shale beds of Barakar involved multiple weathering, erosional, transport, and alterations and basin scale hydro-geologic circulations influenced by shifting of river course and creation of sites for organic deposits through the back-lake system. The studied Barakar shales are significantly organic rich, thermally matured, contains Type III/IV kerogen, having cylindrical, slit to bottle neck pores and encourages the further exploration and development of shales gas in Jharia Basin.

1 STUDY AREA—JHARIA BASIN

The Jharia Basin lies in the heart of Damodar Valley along the north of Damodar River, located in Dhanbad District of Jharkhand State, covering an area of 450 km^2 (Sengupta, 1980). The geological map of the Jharia Basin marked with study area and the cross section along *A–A*' is shown in Fig. 1. The basement of the Jharia Basin is composed of metamorphic rocks overlain by the Talchir Formation followed by Barakar and Barren Measures formations, which are the main shale bearing horizons covering an area of about 218 km^2. The Barakar Formation comprise basal conglomerates, fine to coarse grained and pebbly sandstones, brownish flinty rock, fire clay, shales and coal seams, the cumulative thickness of Barakar shale beds is >100 m. The Barren Measures include carbonaceous shale with ironstone bands, micaceous siltstones and rarely very fine grained sandstones. The Barren Measure is conformably overlain by the shale and coal bearing Raniganj sequence. The rocks of this stage comprise fine to medium grained sandstones-greyish to greenish in colour, siltstones, and carbonaceous shales with thick coal seams. Shale core samples were obtained from Barakar Formation in the eastern part of Jharia Basin during exploratory drilling. A generalized regional chrono-stratigraphic succession of Jharia Coal Field is given in Table 1 (after Coal India Limited, 1993; Chandra, 1992; Sengupta, 1980).

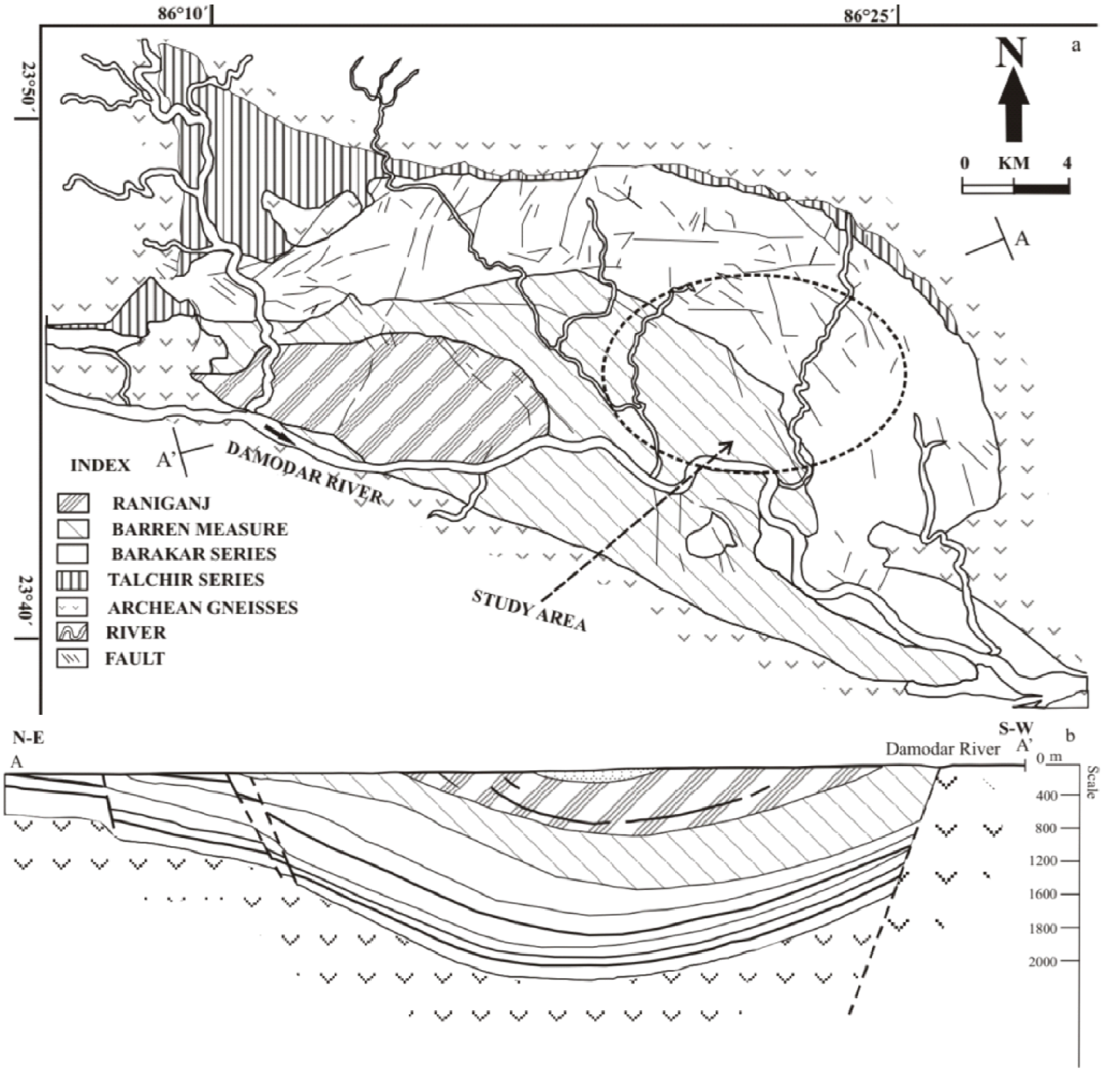

Figure 1. Geological map of Jharia Basin (a) marked location of the study area and (b) cross section along *A–A*' central part of Jharia Basin (after Sengupta, 1980).

Table 1 The generalized stratigraphic succession of Jharia Basin (after Coal Atlas-CMPDI, 1993; Chandra, 1992; Sengupta, 1980).

Age	Group/ Formation		Series/ Epoch	Max. Thickness (m)	Litho-type	Borehole Section
Tertiary to Lower Jurassic	-			-	Dolerites dykes mica lamprophyre dyke and sills	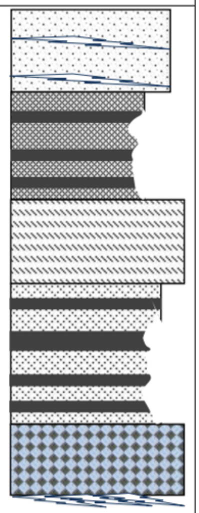
Upper Permian	Damuda Group	Raniganj	Lopingian	800	Fine grained sandstone, siltstones, carbonaceous and grey shale with shale seams	
Middle Permian	Damuda Group	Barren Measures	Guadal-upian	730	Carbonaceous shale with ironstones bands, siltstones and sandstones	
Lower Permian	Damuda Group	Barakar	Cisularian	1250	Buff coloured coarse and medium grained felspathic sandstones, grits, shale, carbonaceous shale and sandstones, shale seams	
Upper Carboniferous	Talchir			245	Fine grained sandstones and greenish shale	
---------------------------------------Unconformity---------------------------------						
Archaean	Meta-morphics			---	Granites, granite-gneiss, quartzite and mica-schist and amphibolites	

2 MATERIALS AND METHODS

2.1 Collection of Borehole Core Samples

In this study, total ten shale core samples were collected from exploratory borehole in the eastern part of Jharia Basin. The studied shale core samples photographs indicating homogenous and banded nature with visible flecks of minerals like quartz and muscovite is shown in Table 2.

2.2 Megascopic and Litho-Band Analysis

The megascopic properties of shale core samples were recorded and vertical as well as horizontal photographs are illustrated in Tables 2 and 3. Shales are characteristically carbonaceous and siliceous type containing variable amounts of clay minerals, quartz/mica flecks and the colour is varying from black to grey. The sub-conchoidal to uneven fractured surfaces were clearly visible in shale core samples. The detailed description about the colour, banding pattern, associated minerals and fossil imprints are given in Table 3. From the detailed litho-band analysis, the dominant lithologies observed are carbonaceous materials, sandstone, siltstone and intercalations and the logs are presented in Table 2.

2.3 Technological Properties and TOC Content

The technological properties of shale/coal or rock is basically the determination of moisture, ash, volatile matter and fixed carbon. Out of four constituent determined under this analysis, the first three are determined experimentally in the laboratory, while the fixed carbon is estimated by subtracting the sum of the total of percentage moisture, ash, and volatile matter from 100 (i.e., fixed carbon=100–(Moist.%+Ash% +VM%). The proximate analysis was carried out following the Bureau of Indian Standards (BIS-1350; Part I, BIS, 1995).

The total organic carbon (TOC) was measured by using a Vinci technologies "Rock Eval 6 Plus with TOC module" instrument to obtain information organic matter content (as weight percent) in the shale core samples. The preliminary cycle of analysis consists of two steps. Firstly, the oven is preset with an initial temperature of 300 °C, which increases to 650 °C at the rate of 25 °C per minute. Released hydrocarbons are studied by a FID (Flame Ionization Detector), forming the so-called peaks S1 (free hydro-carbons from cracking of lipids) and S2 (hydrocarbons from thermal cracking of organic matter). The CO and CO_2 released during pyrolysis can be monitored in real time by an infrared cell. This complementary stage allows determination of total organic carbon content of the samples (Mendhe et al., 2016; Mishra et al., 2014).

2.4 Petrographic Analysis

For petrographic studies, the samples were air dried, manually crushed and sieved to size 0.8 to 1.0 mm for pellet preparation used following International Committee for Coal and Organic Petrology (ICCP, 1998, 1995, 1993, 1973, 1963). The maceral observation was performed on one-side polished pellets with a Carl Zeiss, AXIO Imager M2m microscope at CSIR-CIMFR, Dhanbad using reflected white and fluorescent light as prescribed by ICCP (1993, 1971). All the ten shale samples were analysed for their maceral group and clay and mineral composition. Three major maceral groups have been considered viz., vitrinite, liptinite and inertinite. More than 1 000 points were counted under reflectance and fluorescence attachment with auto-petrolog point counter to have the volumetric composition of maceral group, maceral and mineral matter. The volume percentage of maceral groups and mineral matter are reported in Table 4.

The random reflectance is measured on vitrinite maceral in monochromatic light (wavelength: 546 nm) on Leica DM 4500P microscope, using immersion oil (refractive index: 1.518), 50× objective lens along with a pair of l0× oculars, and Saphire (0.594) along with yttrium-aluminum-garnet (0.904) and gadolinium-gallium-garnet (1.725) as reflectance standards for calibration. microscope photometry system (PMT III) and software MSP 200 is used for the random reflectance measurements and data calculation.

2.5 Low Pressure N_2 Sorption Isotherm

The BET method is used for measurement of adsorption and desorption isotherm points of shale samples using nitrogen as adsorbate at low pressure (<760 mmHg) and isothermal condition maintained with liquid nitrogen (temperature of 77 K) (Sing, 2001). These adsorption and desorption points are used to obtain surface area, pore size and pore volume per mass of the samples (Mishra et al., 2016; Mendhe et al., 2015a; Labani et al., 2013). Quantachrome 'AutosorbiQ^{TM} 2MP-XR' system at CSIR-CIMFR has been used to measure the low pressure N_2 sorption isotherm. The amount of gas adsorbed is evaluated by

Table 2 Facies type and depositional environment of Barakar Formation of Jharia Basin

Litholog/ Samples	Litho-banding schematic	Litho-facies	Weathering/ transport and depositional process	Depositional conditions
	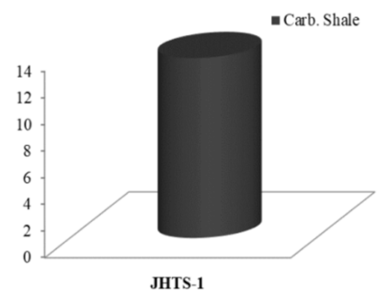	Carbonaceous shale composed of clay, silt and organic matter	Weathering and pedogenesis with low energy sediments alteration	Palaeosol - restricted limno-terrestrial onshore transition
	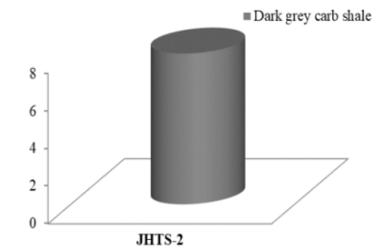	Carbonaceous shale composed of fine to medium grained sandstone interlayers containing mica flakes and sub-angular quartz	Fine interlayered clastic bands developed distally in low lying inter-channel areas of meandering river under low energy environment	The profusion of uni-directional currents under palaeosol - restricted limno-terrestrial onshore transition
	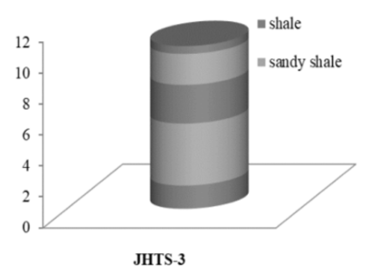	Intercalations containing fine shale to silty clastic laminae, interlayered with laminated carbonaceous shale	Laminated shale of carbonaceous matter with low suspension in fluvial condition corresponding to levee-floodplain deposits	Laminated lenticular shale beds under sandwiched between two or more channels deposition from suspension during low stage

Table 2 Continued

	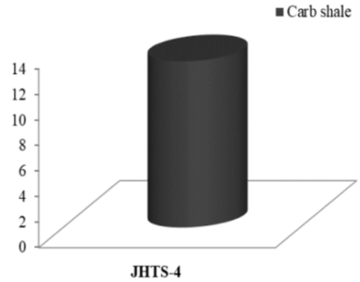	Carbonaceous shale composed of clay, silt and organic matter	Weathering and pedogenesis with low energy sediments alteration	Palaeosol - restricted limno-terrestrial onshore transition
	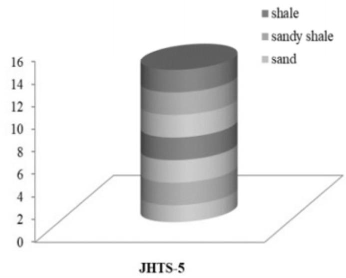	Alternate bands of fine, medium and coarse grained siltstone, clay and organic matter	Planner channel multiple currents transport suggesting intercalation deposits while coarse grained implies rolling of beds	Alternative thin lenticular shale beds deposited mostly from suspension due to velocity currents
	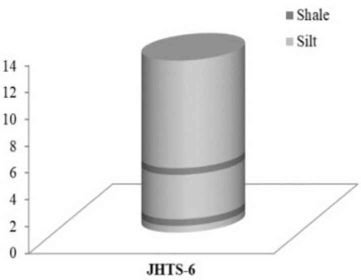	Grey shale, silt and thin bands of carbonaceous matter	The association of thin carbonaceous bands indicates transport and deposition in vertical accretion along the river bank-levee areas of fluvial system	The presence of grey shale with thin stratified carbonaceous matter deposited under low energy condition with irregular fluctuation in energy level

measuring the change of gas pressure. The amounts of adsorptive are introduced successively with the auto system unless it attains equilibrium corresponding to a series of single points on adsorption. It is necessary to pay particular attention to the choice and calibration of the pressure gauges, the verification of adsorption equilibrium and the conditions of out gassing (Rouquerol et al., 1999).

The autosorbiQ is based on the volume of the manifold and hence it is regularly calibrated. The quartz rod, glass calibration tube, spring, O-ring and ferrules are installed. The temperature of the manifold and calibration tube stabilize at the same temperature. The steps suggested by autosorbiQ advanced operation software followed until the confirmation of calibration complete. To ensure accurate temperature readings, the temperature transducer and associated electronics are calibrated with the help of the thermometer, thermocouple calibrator, and calibrated resistors. All the sensors of temperature calibrated following the command prompts on the screen of calibration until confirmation. The pressure transducers are calibrated to ensure accurate readings through its operating range. The 1 000 torr transducers calibrated entering current atmospheric pressure while low pressure transducers are calibrated following the prompts on the screen until confirmation.

The cell containing samples are calibrated along with filler rod without sample (blank analysis). The cell calibration is a blank measurement used to account for the amount of adsorbate gas occupying the cell void volume during the adsorption measurement. After calibration of equipment parts the reference material (alumina-Al_2O_3) having BET surface area 214.15 m^2/g was used for validation.

After satisfactory calibration of the system, about 30 to 40 mg of prepared shale samples (crushed in size of 0.8 to 1 mm) were taken using high precision balance and samples were allowed to outgas at 300 ºC for 3 to 4 h ensuring the removal of bound water adsorbed in the samples. Reagent grade (99.995) N_2 gas was used as adsorbent at liquid nitrogen temperature (-195.79 ºC or 77.35 K), and adsorption-desorption isotherms were obtained under relative pressures (P/Po) ranging from 0 to 0.99 (Quantachrome, 2014). Comprehensive physisorption calculation using single and multipoint BET, Langmuir,

Table 2 Continued

	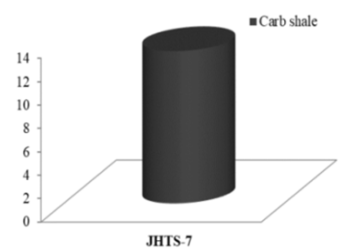	Carbonaceous shale composed of clay, silt and organic matter	Weathering and pedogenesis with low energy sediments alteration	Palaeosol - restricted limno-terrestrial onshore transition
	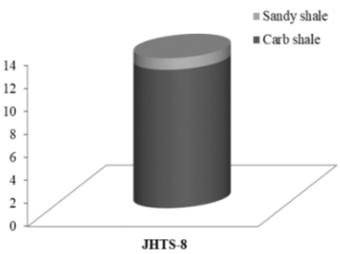	Sandy and carbonaceous shale with fine to medium grained silt, visible tiny flakes of muscovite and quartz	Weathering and transport under low suspension currents chiefly uni-directional in an abundant channel fill	The upward coarsening material states asymmetric channel currents due to decline of current velocity in fluvial system
	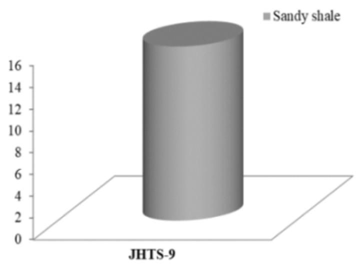	Sandy shale with coarse grain of muscovite, quartz and feldspar, in between discrete laminae of very thin dispersed organic matter	Laminated striations indicating regular geometry indicates sediment deposited in a vertical accretions under fluvial system	Massive sandy shale with stratified laminations of feldspathic laths suggests differential transport in a channel due to fall in energy of deposition
	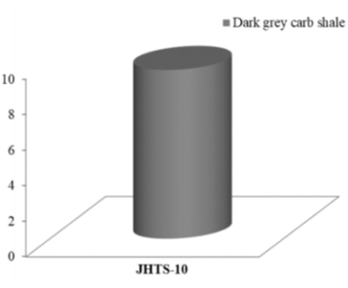	Carbonaceous shale composed of clay, silt and organic matter	Weathering and pedogenesis with low energy sediments alteration with reducing environment	Palaeosol - restricted limno-terrestrial onshore transition followed by fluvial system

Table 3 Megascopic and technological properties of Barakar shales in Jharia Basin

Sample No.	Depth (m)	Rock type	Ash (wt.%)	IM (wt.%)	VM (wt.%)	FC (wt.%)	S1	S2	T_{max}	TOC (wt.%)	HI	Physical properties
JHTS-1	102.50	Carbona-ceous shale	73.04	0.77	10.68	15.51	3.27	21.14	462	17.32	122	Black to grey, sub-conchoidal to uneven fracture, fossil imprints
JHTS-2	72.50	Carbona-ceous shale	86.31	1.32	8.33	4.04	0.79	9.82	454	6.81	144	Dark grey, massive, uneven fracture, mica and quartz flecks
JHTS-3	60.50	Banded shale	80.71	1.37	10.5	7.42	0.92	4.82	436	9.36	51	Alternative bands of silt and clay, uneven fracture, fossil imprints, fine grained mica, feldspar and quartz
JHTS-4	116.00	Shale	75.10	1.12	10.88	12.90	2.27	20.54	468	14.65	140	Laminated alternate bands of silt and clay, flecks of mica and quartz
JHTS-5	14.50	Sandy shale	88.07	1.23	7.91	2.79	0.49	1.82	364	3.15	58	Dark grey, alternate band of carbo-naceous material, silt and clay, flecks of mica and quartz
JHTS-6	122.00	Sandy-silty shale	91.89	0.93	4.33	2.85	0.35	2.58	438	4.08	63	Uneven to sub-conchoidal fracture, fossil imprints, laminated bands of silt and sand
JHTS-7	81.50	Carbona-ceous shale	76.84	1.05	10.46	11.65	1.27	18.14	466	14.25	127	Uneven to sub-conchoidal fracture and slicken slide
JHTS-8	84.50	Sandy shale	91.44	0.92	5.34	2.30	0.42	6.17	439	2.78	222	Uneven to sub-conchoidal fracture, intercalations, minor grains of mica and quartz
JHTS-9	39.50	Sandy shale	85.97	1.29	11.76	0.98	0.12	5.87	442	1.67	351	Light grey, intercalations in between carbonaceous material, uneven fracture
JHTS-10	54.50	Shale	91.14	0.62	7.73	0.51	0.18	0.29	444	1.21	24	Alternate bands of silts and intercala-tions, uneven to sub-conchoidal fracture, minor grains of mica and quartz

S1. Free hydrocarbons in sample (mg HC/g rock); S2. remaining hydrocarbons (mg HC/g rock); T_{max}. maximum temperature of pyrolysis (°C); TOC. total organic carbon (wt.%); HI. [(S2/TOC)×100] hydrogen index (mg HC/g TOC).

Table 4 Maceral and mineral matter composition of shale core samples

Sample No.	Vitrinite (vol.%)	Liptinite (vol.%)	Inertinite (vol.%)	Mineral matter (vol.%)			Total mineral matter (vol.%)	Vitrinite reflectance (%)
				Quartz	Muscovite	Clay		
JHTS-1	12.98	3.23	9.05	12.49	6.77	55.48	74.74	1.23
JHTS-2	5.32	1.03	2.91	2.32	6.38	82.03	90.74	0.76
JHTS-3	7.34	0.17	1.80	0.36	6.10	84.23	90.69	0.85
JHTS-4	11.51	1.29	0.96	0.98	2.70	82.57	86.24	1.26
JHTS-5	1.85	0.34	0.42	1.61	2.81	92.96	97.39	0.76
JHTS-6	3.97	0.70	0.23	0.56	3.91	90.64	95.10	1.19
JHTS-7	10.89	1.33	2.34	0.38	1.09	83.98	85.44	1.02
JHTS-8	0.86	0.32	0.68	0.46	3.41	94.27	98.14	0.96
JHTS-9	0.28	0.23	0.39	10.78	0.32	88.00	99.10	0.92
JHTS-10	0.81	0.76	0.56	0.65	0.85	96.37	97.87	0.78

BJH, DFT, DR, DA and t-plot methods were carried out to determine surface area, pore size distribution and pore volume of shale samples (Mendhe et al., 2017a, b, 2015b; Mishra et al., 2016; Kuila et al., 2012).

3 RESULTS AND DISCUSSIONS

3.1 Megascopic and Technological Properties

The studied shale core samples obtained from Barakar Formation in Jharia Basin laterally varying depth from 14.50 to 122 m, black, dull, dark to light grey in colours, typically composed of variable amounts of clay/mud and minerals like quartz and mica flecks, however, alternate bands of silt/clay and incoherent amounts of minor constituents alters the colour of the shales. The detailed description about the colour, banding pattern, associated minerals, and fossil imprints are given in Table 3. The fractured surfaces of samples are sub-conchoidal to un even. The black to grey shale results from the presence rich carbonaceous material (organic content) and deposited in low-energy fluvio-lacustrine waters in reducing environment. It is accentuated that the organic-rich nature of the shale, along with its high degree of lamination suggests anoxic waters that protected the organic material from decay, while its clay content is high, makes the shale relatively massive, which is likely effect on the response of the shale to hydraulic fracturing. The megascopic photographs of the shale core samples are given in Table 2.

Results of technological properties of shale core samples determined following the Bureau of Indian Standard (IS:1350; BIS, 1995) on air-dried basis is given in Table 3. It includes moisture, ash, volatile matter and fixed carbon content likely varies from 0.62 wt.% to 1.37 wt.%, 73.04 wt.% to 91.89 wt.%, 4.33 wt.% to 11.76 wt.%, and 0.51 wt.% to 15.51 wt.%, respectively. The high ash content is confirming the dominance of minerals in the studied shale samples. The distribution of technological properties with depth of the shale core samples is shown in Fig. 2. The values of total organic carbon (TOC) varying from 1.21 wt.% to 17.32 wt.%, signifying excellent source rock potential, the similar observations are made by Mani et al. (2015) for Jharia shales. The TOC ranges are similar to that of the Chang 7 shale of Yanchang Formation Ordos Basin in China presented by Zhao et al. (2017). The relationships between fixed carbon with the depth show that the maturity of the shale spans the reduction in volatile matter and raise in carbon content with depth of burial of shale beds (Fig. 3, correlation coefficient R^2=0.274 7), which is the most widely accepted indices of maturity of shale or coal. The usual decline trend of fixed carbon with increasing ash percentage is shown in Fig. 4 (R^2= 0.901).

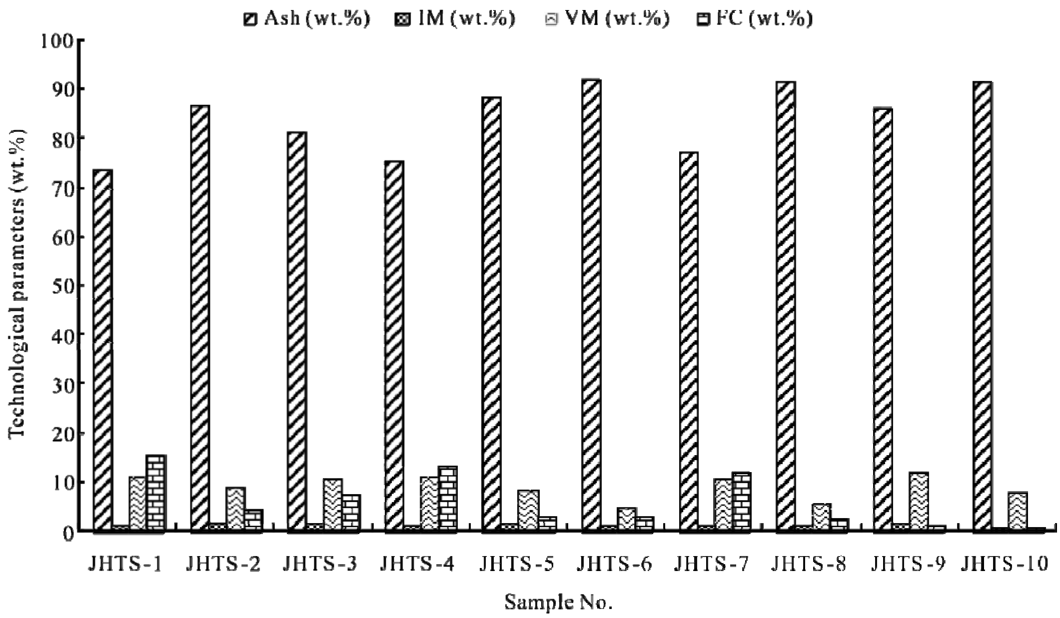

Figure 2. Distribution of technological parameters in shale cores samples.

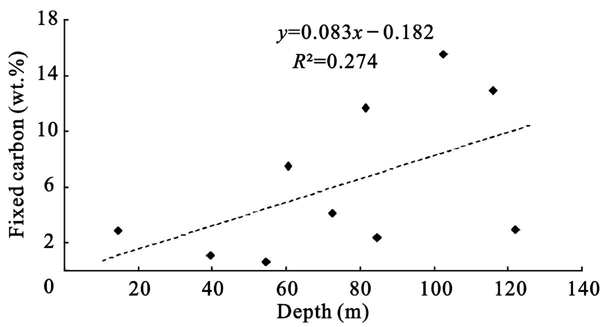

Figure 3. Increasing trend of fixed carbon with depth.

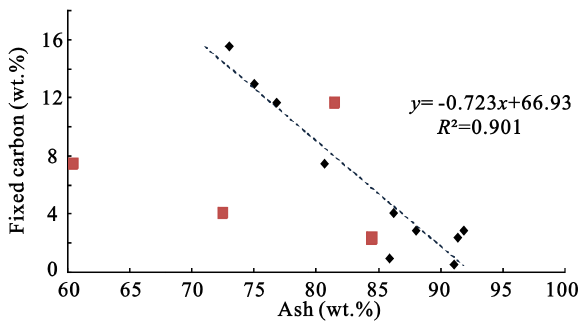

Figure 4. Declining trend of fixed carbon with ash content.

3.2 Facies-Depositional Environment

The core samples describing litho-bands of carbon rich, silt, clay-sericite, intercalations and sandy shales containing coarse grained visible discrete sub-angular quartz and mica flecks along the laminae, signifies the mode of heterogeneity, transport and depositional process for shale deposits. Table 2 shows the vertical and horizontal section of core samples describing facies type and depositional environments of Barakar shale beds. The studied samples are placed, according to the occurrence in borehole, elucidating low energy sediments numerously altered under reducing environment. It is found that the massive nature of carbonaceous and silty shale presenting profusion of uni-directional currents under palaeosol-restricted limno-terrestrial-fluivial onshore transition bedding characteristics (Sen et al., 2016; Jacob et al., 1958). The significant amount of angular to sub-angular grains of quartz makes shale beds detrital nature may favour artificial hydrofrac during well completion. Though, the degree of sorting is less among the samples point towards the homogenous nature of shale beds, therefore a larger proportion of the grains are finer-clay than the silt and grit. The intricate microstructures, fractures and tapered matrix resulting poor pore connectivity influenced by osmotic effects on clays and mineral alteration (Roshan et al., 2016; Singh, 2016).

The study of source material of Barakar shale deposits, signifies mineral constituents are derived from granitic rocks, however, the sericite-clay and the associated mineral grains have been contributed by low grade metamorphic rocks during the weathering, erosion and pre-post digenetic process, similar opinions also noted by several authors (Chandra, 1990; Chandra and Betekhtina, 1990). The lithofacies, weathering, transport, depositional process and environment demonstrating Barakar shales were sorted and deposited under quitter, irregular low energy and fluvial conditions, similar observation recorded by several researchers (Chandra, 1992; Casshyap and Tewari, 1987; Tewari and Casshyap, 1982; Jacob et al., 1958). According to Tewari and Casshyap (1983), Casshyap (1970), the channel shaped fine grain siltstone and shale beds are the results of attributed largely to channel shifting corresponds to levee deposits of the meandering stream under reducing fluviatile-fresh water conditions acted by Damodar River. According to Chandra (1992), during Lower Permian, the process of river course changes created back swamp areas favourable for coal seam deposits.

It is concluded that the content of organic matter is inversely proportional to sedimentation level, thus the rate of accumulation of organic carbon were similar in carbonaceous shale beds (USGS, 1986). However, the type of organic matter deposits in shale beds controlled by reduction in intensity of anaerobic diagenesis and by the influence of terrestrial organic matter. The facies briefs the evolutionary trend of basin sediments, the cycle of weathering, erosion and sedimentation process causing changes in composition pointed by striations (Table 2). The chiefly clay content indicating terrestrial-fluvial facies. According to Brooks (1952) and Grim (1947), the abundance of clay minerals in shale help to concentrates organic constituents by adsorbing the source material, consequently behaving as catalysts in hydrocarbon generation and accumulation. However, clay minerals in large shall have an impact over porosity and permeability required for gas flow in the reservoir. The dissolution of clay, due to diagenetic processes may block the secondary porosity and cause the reduction in permeability.

3.3 Petrographic Controls on Reservoir

The results of petrographic analyses containing maceral composition and mineral matter determined on volume percentage are exhibited in Table 4. The vitrinite, liptinite, inertinite and mineral matter values are measured in the range of 0.28 vol.% to 12.98 vol.%, 0.17 vol.% to 3.23 vol.%, 0.36 vol.% to 9.05 vol.%, and 74.74 vol.% to 99.10 vol.%, respectively, however, mineral matter is further subdivided into chiefly appearing minerals like quartz, muscovite and clays varies from 0.36 vol.% to 12.49 vol.%, 0.32 vol.% to 6.77 vol.%, and 55.48 vol.% to 96.37 vol.%, respectively. The petrographic analysis also focused by means of the origin of the constituents, texture-layout and distribution of grains, the degree in which they fill the rock spaces, structure and orientation of grain size and shape, pore and hair fracture space characteristics and interconnections of empty voids. It is observed that shales are frequently very heterogeneous during microscopy. The micro-photographs of maceral present within the shale samples are given in Fig. 5.

The organo-petrographic study shows vitrinite as dominant maceral followed by inertinites and liptinites with inorganic minerals like quartz, muscovite, pyrite and clays (kaolinite/sericite). The usually observed inertinites are funginite, semifusinite and fusinite, while the inputs of liptinite maceral like alginite and sporinite pointing towards proneness of gas genesis potential of shale. The macerals of vitrinite group such as tellinite (Fig. 5g), collotellinite, and vitroderinite are differentiated on the basis of the presence and absence of the textural features structures and their size. The macerals collotellinite is homogeneous in appearance whereas tellinite shows well preserved cell structures where cell lumens are either filled with colliniteor clay minerals. When collotellinite occurs in particulate form (<10 μm in size> it is characterised as vitrodetrinite (Taylor et al., 1998) (Fig. 5a). Liptinite macerals are characterized by dark gray to black colour in low rank shale with distinct morphology (Fig. 5d). The liptinite macerals are sporinite, alginite, and liptodetrinite. It is characterized by more or less lens shaped in section perpendicular to the bedding cavity appear as thin line, size of sporinite can vary from 5 to 350 μm. Inertinite is branded by well-preserved cell structure and shape of cavities vary in size and shape being more commonly round, oval or elongated, yellowish white to white colour with very high reflectance and strong relief (Figs. 5c, 5e). The macerals emifusinite distinct as a stage between fusinite and telocollinite/collotelinite, cell structure is less well defined as compared to fusinite (Fig. 5b).

The maceral composition of the shale has been studied in detail, in order to obtain a microfacies classification and to deduce palaeo-environments during shale deposition. The volumetric percentages of the three maceral groups, vitrinite, inertinite and liptinite are presented in ternary diagram (Fig. 6) in order to provide the fundamental information on thermal maturity. It is substantiated that Barakar shales of Jharia are vitrinite rich and placed in thermal-dry gas prone region, Type IV kerogen (Fig. 6) (Mendhe et al., 2016; Mishra et al., 2016; Hakimi et al., 2013; Tissot and Welte, 1978).

The amalgamation of diagenetic and depositional conditions revel heterogeneity in shale beds mineralogy controlling the percentage of clay, quartz, feldspar, muscovite and other detrital mineral grains. The ternary plot of mineral distribution illustrating weathering pattern of Barakar shale beds in Jharia and likely influence on porosity and permeability as given in Fig. 7. The studied shale samples belong to high porosity and

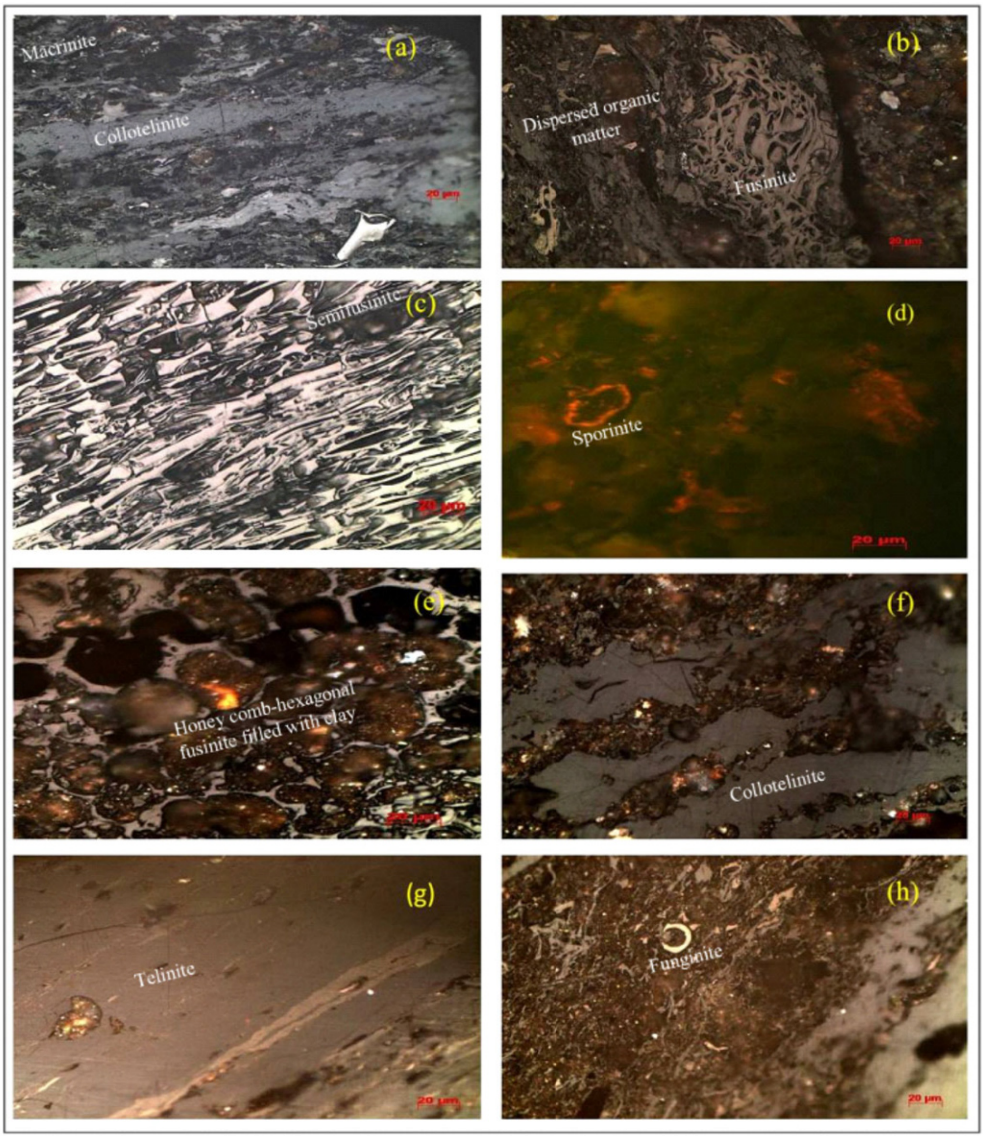

Figure 5. Micro-photographs of Barakar shale core samples of Jhraia Basin. (a) Collotelinite-vitrodetrinite and macrinite (JHTS-1); (b) fusinite bounded by clay and disbursed organic matter (JHTS-1); (c) semifusinite showing elongated pores (JHTS-1); (d) sporinite-liptodetrinite imbedded in vitrinite and clay/mud (JHTS-2); (e) fusinite with distinct hexagonal pore filled with clays/muds (JHTS-2); (f) collotellinite laths interbred by micrinite and clays in ground mass (JHTS-4); (g) telinite with elongated macro- and meso-pores (JHTS-4); (h) funginite and disbursed vitrinite (JHTS-7).

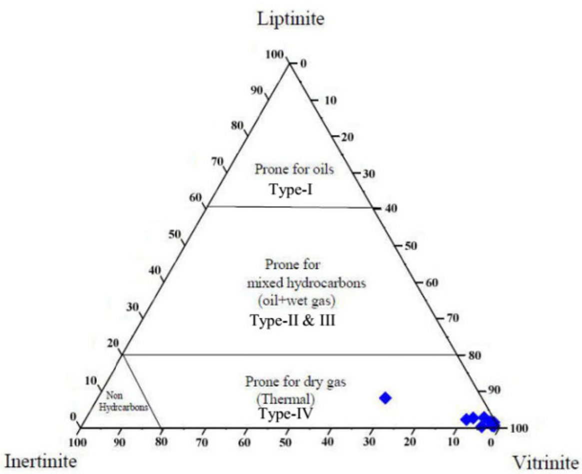

Figure 6. Ternary diagram of maceral distribution illustrating Barakar shale of Jharia are placed in thermal-dry gas prone region.

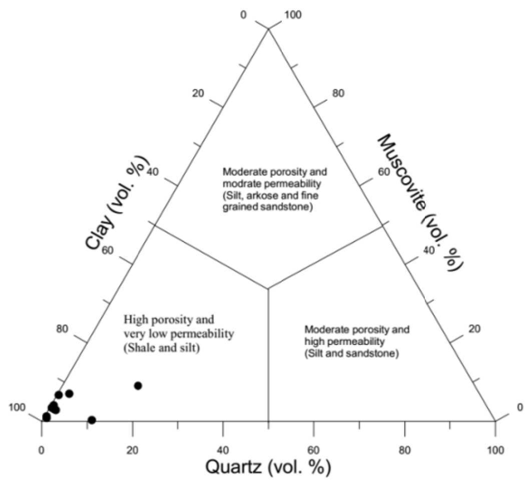

Figure 7. Ternary diagram of mineral distribution showing likely porosity and permeability based on weathering pattern of deposition.

very low permeability pointing towards dominance of clay and silts. The formation of shale beds containing chiefly clays from granitic and feldspathic rocks occurred in Damodar Valley Basin is the result of multiple weathering, erosional, transport, alteration during post depositional process and basin scale hydro-geologic circulation, Several authors reported that the secondary alteration and dissolution affects the porosity and permeability through blocking effects (Person et al., 1996; Winstch et al., 1995; Moore et al., 1982).

The contribution of different macerals in total organic content shown in Fig. 8, indicating positive correlations with the macerals however, vitrinite content largely contributing in TOC as well as in types III and IV kerogen. It is concluded that thermally matured vitrinite and inertinite are the major source of gas generation and the potential source rock (Wei et al., 2016; Mastalerz et al., 2012a). The negative correlation of TOC and clay content (R^2=0.641) shown in Fig. 9 implies that sedimentation of clays occurred mostly by change in channel position, which affects continuity of organic deposits at the similar location while enhances the degree of decomposition of organic matter as a result TOC preservation diminishes. However, large amount of clays derived from K-feldspar causing reduction of permeability, because of intensive early and post diagenetic carbonate and silicates cementations. Hence, it is interpreted that organic matter content significantly affected during alteration of hydrocarbon compounds influenced by terrestrial

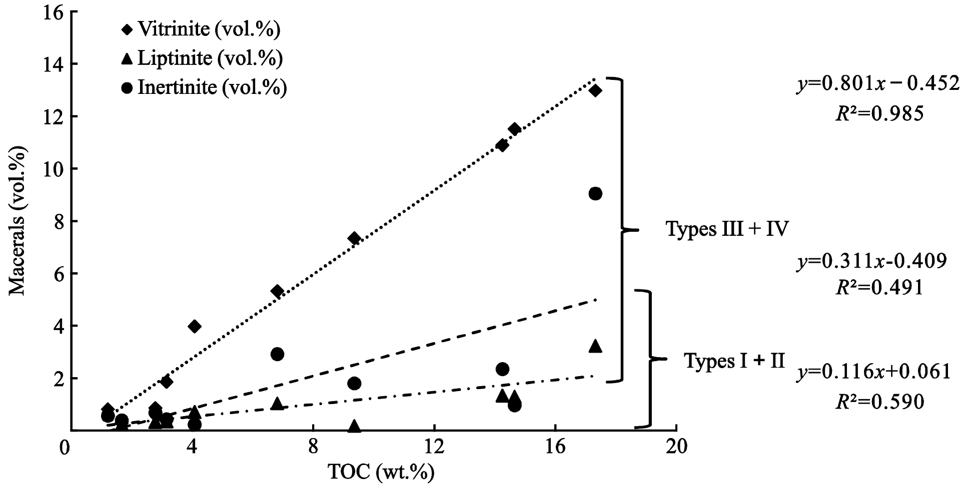

Figure 8. Relation of total organic content with vitrinite, liptinite and inertinite.

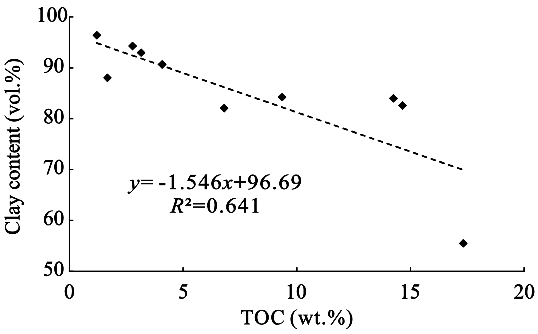

Figure 9. Relation of total organic content with clay content.

hydrologic cycles (Uysal et al., 2004).

3.4 Pore Facets and Their Implications on Methane Storage

The low pressure N_2 sorption isotherm is used to determine the amount of gas adsorbed and desorbed at different relative pressure (P/P_o), where P is the gas vapour pressure in the system and P_o is the saturation pressure of adsorbent. The Quantachrome Autosorb system has given the adsorption isotherm points by measuring nitrogen adsorbed quantity and the equilibrium pressure, while desorption isotherm obtained by measuring the quantities of released from the sample as the relative pressure is lowered. The adsorption isotherm curves are grouped into five types (types I to V) (Quantachrome, 2014; Brunauer et al., 1940, 1938). The results of surface area, pore size and pore volume obtained through low pressure N_2 sorption isotherm is given in Table 5.

The surface area determined by methods like multipoint BET, Langmuir, BJH, DFT and DR is varying from 2.60 to 11.31, 4.40 to 19.28, 1.57 to 4.99, 1.98 to 8.60, and 2.08 to 11.85 m^2/g, respectively (Figs. 13 and 15). The pore size distribution obtained using BJH, DFT, DA, DH, DR and average pore diameter ranges from 2.98 to 3.95, 3.92 to 3.97, 1.58 to 1.84, 2.98 to 3.95, 1.45 to 1.94, and 6.12 to 11.01 nm, respectively (Table 4), indicating that the studied Barakar shales are mostly mesoporous. According to IUPAC (1997) pore size classification is such as micropore <2 nm, mesopore 2–50 nm and micropore diameter >50 nm. The low pressure N_2 sorption curve obtained (Fig. 11) have been correlated with different types of hysteresis loops illustrated by de Boer (1958), Labani et al. (2013) (Fig. 10). Type A hysteresis corresponds to cylindrical pores; Type B is related to slit-shaped pores; types C and D hysteresis are attributed to wedge-shaped pores, and Type E hysteresis is produced by bottle neck pores.

It may be observed that low pressure N_2 isotherms are mostly Type II curve and shows H2 type of hysteresis pattern (Fig. 11). Type II curve shows presence of non-porous to macro-porous adsorbent and also indicate both monolayer-multilayer adsorption. The hysteresis H2 pattern represents the presence of dis-ordered and the distribution of pore size and shape is not well defined. Hence, the observation shows that Barakar shales are heterogeneous in nature for their pore structure, cylindrical, slit and bottle neck pores, which may be owed to wide range of organic and clay content (Mendhe et al., 2017a, b; Wang M et al., 2015; Clarkson et al., 2012).

The plots of multipoint BET are presented in Fig. 12, showing variations in surface area due to heterogeneity of pore size distribution controlled by organic and inorganic content of shales. Figure 13 exhibits the BJH plots indicating dominance of mesopores in studied shales, these plots are also been used for estimation of surface area, pore size distribution and pore volume in shale core samples. The pore volume of shales acquired following BJH, DFT, t-method (micropore volume), DH, DR and total pore volume varies from 0.007 to 0.013, 0.005 to 0.015, 0.001 to 0.002, 0.006 to 0.013, 0.001 to 0.004, and 0.007 to 0.017 cc/g, respectively. To calculate pore size distribution, the application of the BJH model to the desorption branch of the isotherm that is characterized by a hysteresis loop of type H2 or H3 (Sing et al., 1985) is often much more affected by pore network effects than the adsorption branch.

The distribution of pore volume with respect to pore size can be displayed as cumulative, incremental or differential distribution curves (Kuila and Prasad, 2013; Clarkson et al., 2012; Mastalerz et al., 2012b; Meyer and Klobes, 1999). The cumulative curve is a plot of pore volume vs. pore diameter from which a differential distribution may be obtained by differentiation. A plot of the derivative of pore volume with respect to pore diameter, i.e., dV/dW versus W, is referred to as the differential distribution plot and the pore volume in any pore width range is given by the area under the curve (Fig. 13). It is clear that the pore distribution derived from the desorption branch of the isotherm shows a strong artificial pores peak at approximately 4 to 10 nm while the selection of the adsorption branch for pore size calculations indicates the absence of the well-defined distribution pores, and has shown a much broader distribution. DFT plots for determination of surface area, pore size and pore volume of shale core samples are given in Fig. 14. Both the BJH- and DFT-derived pore diameter illustrated that the pore volumes are mainly controlled by larger pores, but the surface areas are mainly contributed by smaller pores.

3.5 Controls of Depth of Occurrence

In general, depth of occurrence of shale reservoir controls the preservation of organic matter, maturity, storage and transport mechanism. Figure 15a, shown slightly increase in TOC content with increase in depth (R^2=0.239 7) indicating organic richness of Barakar shales in Jharia Basin. However, small values of correlation coefficient signifies organic matter in shales affected due to biodegradation near the surface, while preserved at greater depth under reducing environment, transforming into higher kerogen type, similar observation recorded by Alsharhan and Nairn (2003). According to Mani et al. (2015), the Barakar shales of Jharia Basin have experienced significant maturity and increases with depth. The negative trend of surface area with depth (R^2=0.217), signifying alteration and dissolution of clays, carbonates and silicates blocking the pore opening, which do not allow the N_2 gas to enter and

Table 5 Results of surface area, pore size and pore volume obtained from low pressure N_2 sorption isotherm of shale core samples

Sample No.	Surface area (m^2/g)						Pore diameter (nm)						Pore volume (cc/g)					
	Multi point BET	Single point BET	Langmuir	BJH	DFT	DR	BJH	DFT	DA	DH	DR	Avg. pore	BJH	DFT	t-Method	DH	DR	Total pore volume
JHTS-1	3.49	3.280	5.94	2.03	2.72	2.94	3.32	3.97	1.80	3.32	1.89	8.53	0.007	0.006	0.00	0.006	0.001	0.007
JHTS-2	11.31	10.85	19.28	4.99	8.60	11.85	3.13	3.92	1.72	3.13	1.94	6.12	0.013	0.015	0.002	0.013	0.004	0.017
JHTS-3	4.34	4.13	7.35	2.43	3.21	3.78	3.15	3.95	1.84	3.15	1.92	8.83	0.008	0.007	0.00	0.008	0.001	0.010
JHTS-4	2.60	2.48	4.40	1.57	1.98	2.08	3.95	3.96	1.68	3.95	1.58	11.01	0.007	0.005	0.00	0.006	0.001	0.007
JHTS-6	4.85	4.64	8.19	2.27	3.71	4.09	2.98	3.99	1.58	2.98	1.45	7.26	0.007	0.007	0.001	0.007	0.001	0.009
JHTS-9	6.55	6.28	10.65	2.96	4.75	6.59	2.98	3.92	1.70	2.98	1.80	7.77	0.010	0.010	0.001	0.010	0.002	0.012

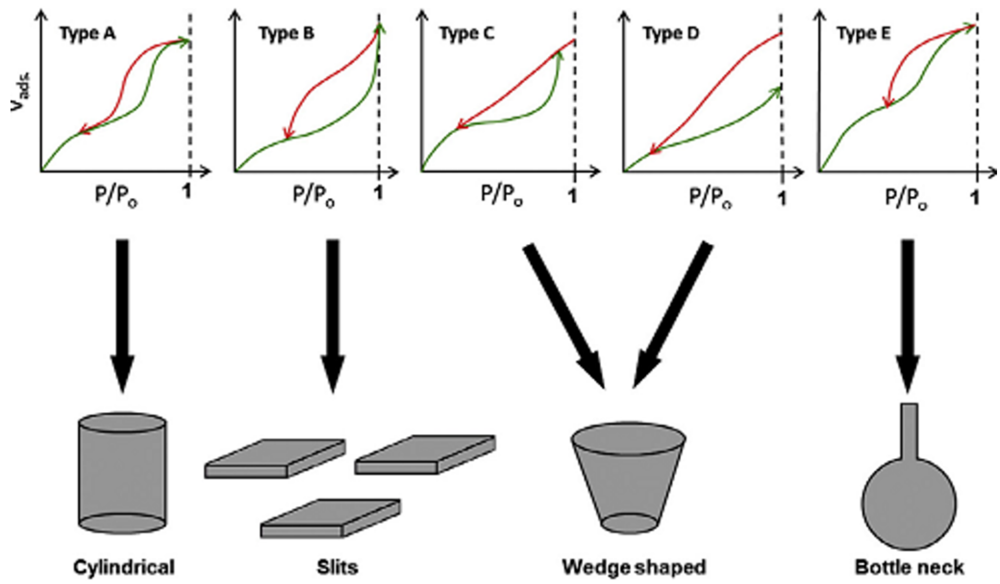

Figure 10. Different types of hysteresis pattern representing their pore geometrical shapes (after Labani et al., 2013; de Boer, 1958).

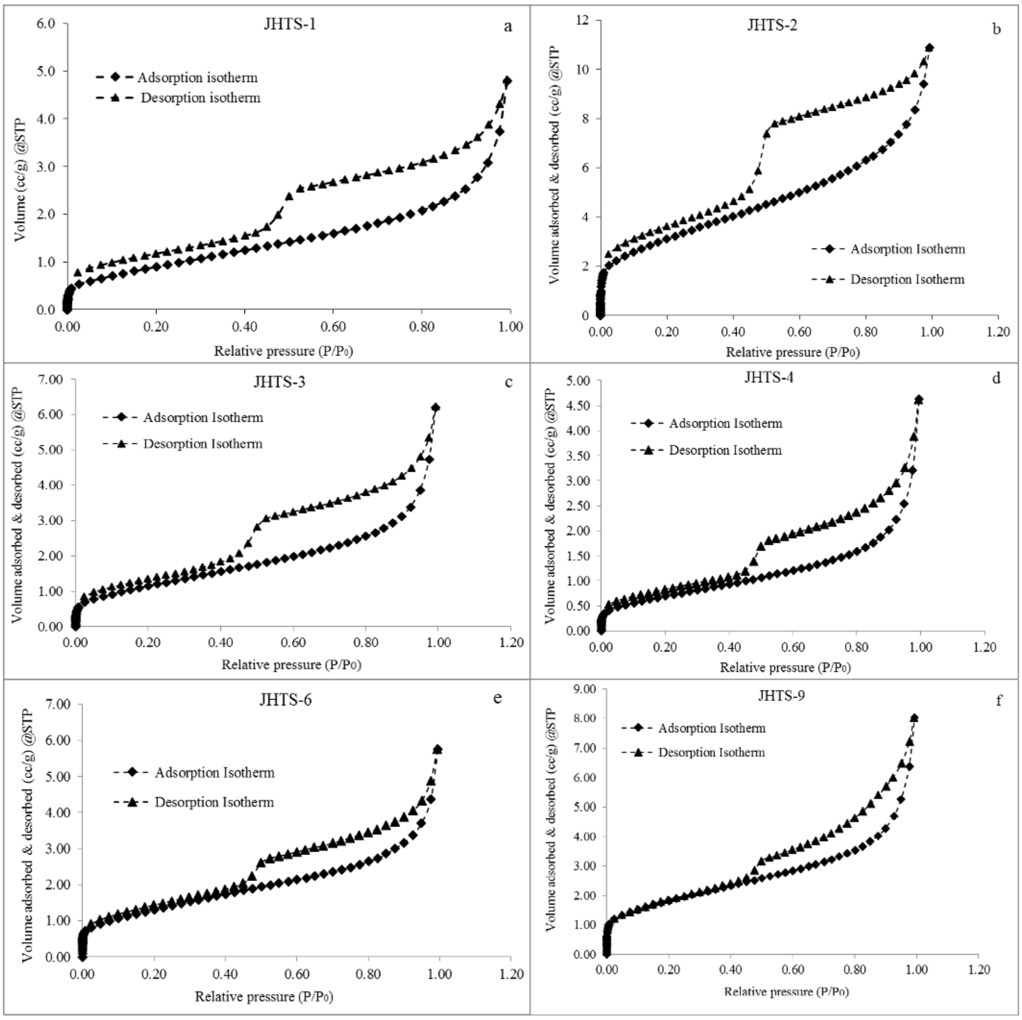

Figure 11. Low pressure N_2 sorption isotherm of Barakar shale core samples (a) cylindrical-type A; (b) large spaced open slit pores-type B; (c) cylindrical-type A; (d), (e) and (f) bottle neck-type E.

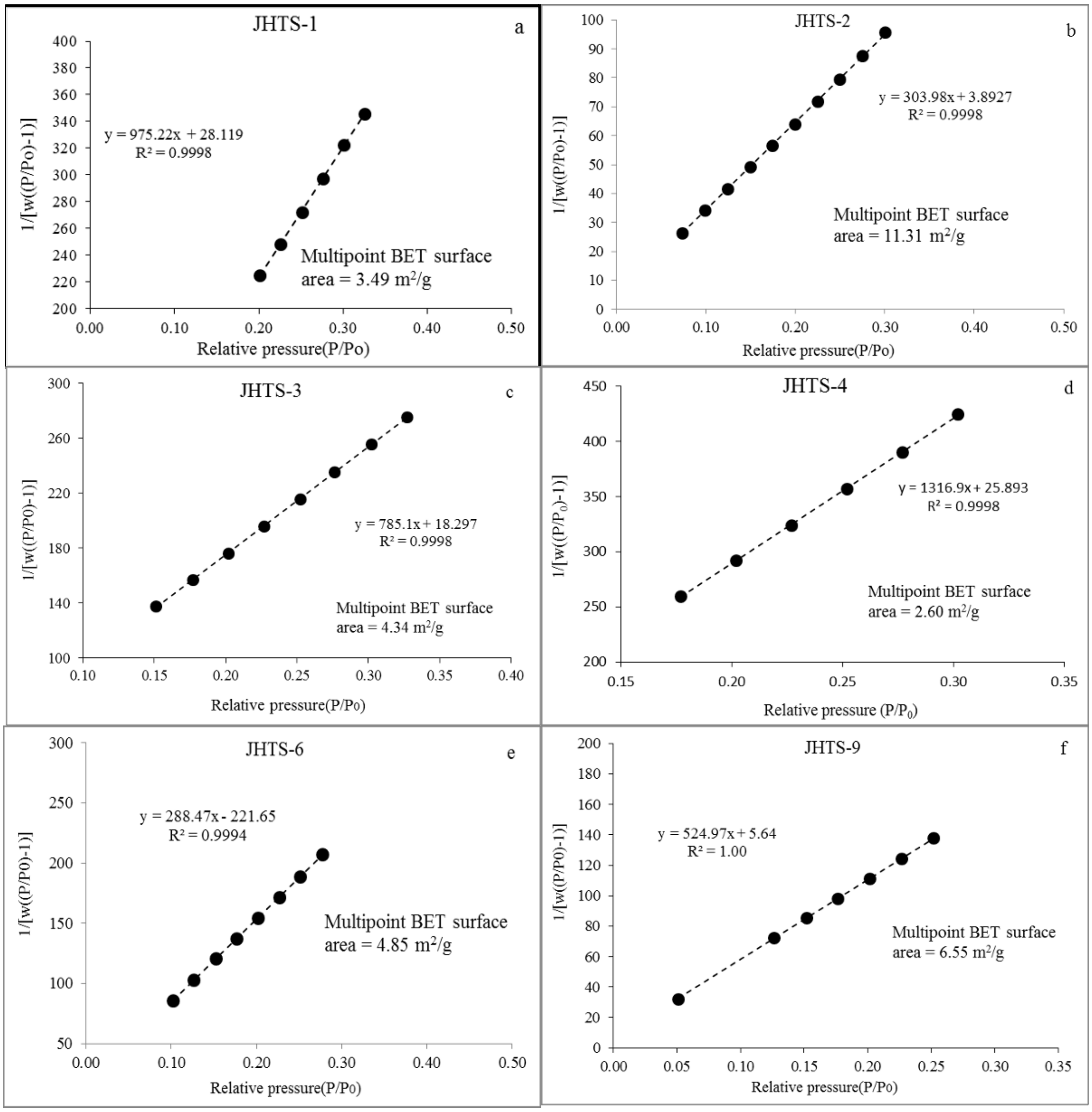

Figure 12. Multipoint BET plots for surface area determination of shale core samples.

adsorbed, hence surface area get reduced (Mendhe et al., 2017a, 2015b). The size of pores increases with increase in overburden pressure, specifying basin tectonics and re-structuring accountable for creation of secondary or meso to macro pores in shale beds (Fig. 15c) (Chalmers and Bustin, 2007). This leads to reduction in pore volume, because larger pores have less pore volume compared to smaller pores (Fig. 15d) (Mendhe et al., 2017a, b; Mishra et al., 2016).

3.6 Controls of Thermal Maturity

The vitrinite reflectance is the maturity parameter used for coal or shale dispersed organic matter for evaluation of source rock, relating to transformation of kerogen due to temperature effects (Pophare et al., 2008; Durand et al., 1986). The results of vitrinite reflectance measured randomly varies from 0.76% to 1.26%, signifying thermally matured shales prone for dry gas genesis (Mendhe et al., 2016; Mishra et al., 2016; Varma et al., 2015). The plot of vitrinite reflectance and varying depth is given in Fig. 16a, illustrating excellent correlation (R^2=0.710 8) suggests that like coal, shale beds carbonaceous matter also controlled by depth of occurrence. As a result, deeper shale beds are relatively less weathered and preserved organic matter functioned as gas genesis source. The positive correlation of TOC and vitrinite reflectance (R^2=0.389 3) pointing usual trend of matured material containing higher organic carbon (Fig. 16b) (Mendhe et al., 2017c, d). Figure 16c shown the very good negative correlation of surface area and V*R*o (R^2=0.606 6), indicating influence of vertical stresses and thermal maturity compacted the shale beds in massive form, destroyed pore structures, fractures and free spaces. However, size of pore increases with vitrinite reflectance, implies thermal cracking of kerogen and repulsion of volatiles generated larger mesopores of size 2.98 to 3.95 nm (Fig. 16d). The plot of S2 vs. TOC shows that hydrocarbons released is characterized as dominantly presence of Type III/IV gas-prone kerogen in the Barakar shales (Fig. 16e), similar interpretations also recorded by Mani et al. (2015). The values of T_{max} ranges between 364 to 468 ºC (Table 3), signifying matured source rock, except Sample JHTS-5 obtained from least depth (14.50 m). Figure 17f, shown T_{max} vs. HI of shale samples, demonstrating condensate-wet to dry gas window and hence falling within mature stage (Mendhe et al., 2017a; Mani et al., 2015; Varma et al., 2015).

3.7 Controls of TOC on Pore Features

The multipoint BET surface area and pore volume showed weak negative correlation with TOC (R^2=0.285 2 and 0.280 8), signifying that the organic matter content does not play major role in the of storage gas in the studied shale samples (Figs. 17a and 17b). The decline of surface area may be due to the abundance of disintegrated minerals, although, sudden increase in temperature and pressure caused cracking of organic matter and destruction of pores which would have reduced the association of organic pores in surface area (Mendhe et al., 2017a, b, c, d; Li et al., 2016; Wang M et al., 2015; Curtis et al., 2012). The relationship between pore size and TOC content showed the collective trend (R^2=0.532 4) (Fig. 17c) suggesting that thermal evolution of organic matter affects the complexity and heterogeneity of pore size and structures, as a results pore size increases (Fu et al., 2017; Li et al., 2016). The pore volume mostly dependent on pore size and structures shale beds influenced by organic and inorganic matter. Figure 17d, emphasized that fixed carbon do not contribute to smaller pore formation compared to clay and other minerals.

4 SUMMARY AND CONCLUSION

The Barakar Formation of Jharia Basin have been evaluated for shale gas reservoir characteristics focusing on organo-petrographic and pore facets controlled by depositional environment and different geological parameters. The black to grey shale bed of Barakar Formation resulted from low-energy fluvio-lacustrine waters in reducing environment containing high carbonaceous material (organic content). However, high degree of lamination suggests anoxic waters that protected the organic material from decay, though high clay content makes the shale relatively massive, whereas moderate quartz content, likely make the shale beds brittle and may favour during hydraulic fracturing. The volatile matter reduction and increased in TOC content with depth have been observed. The maceral composition based facies substantiated that Barakar shales of Jharia are vitrinite rich and placed in thermal-dry gas prone region. The shale beds of Barakar Formation are the results of multiple weathering, erosional, transport, and alteration during

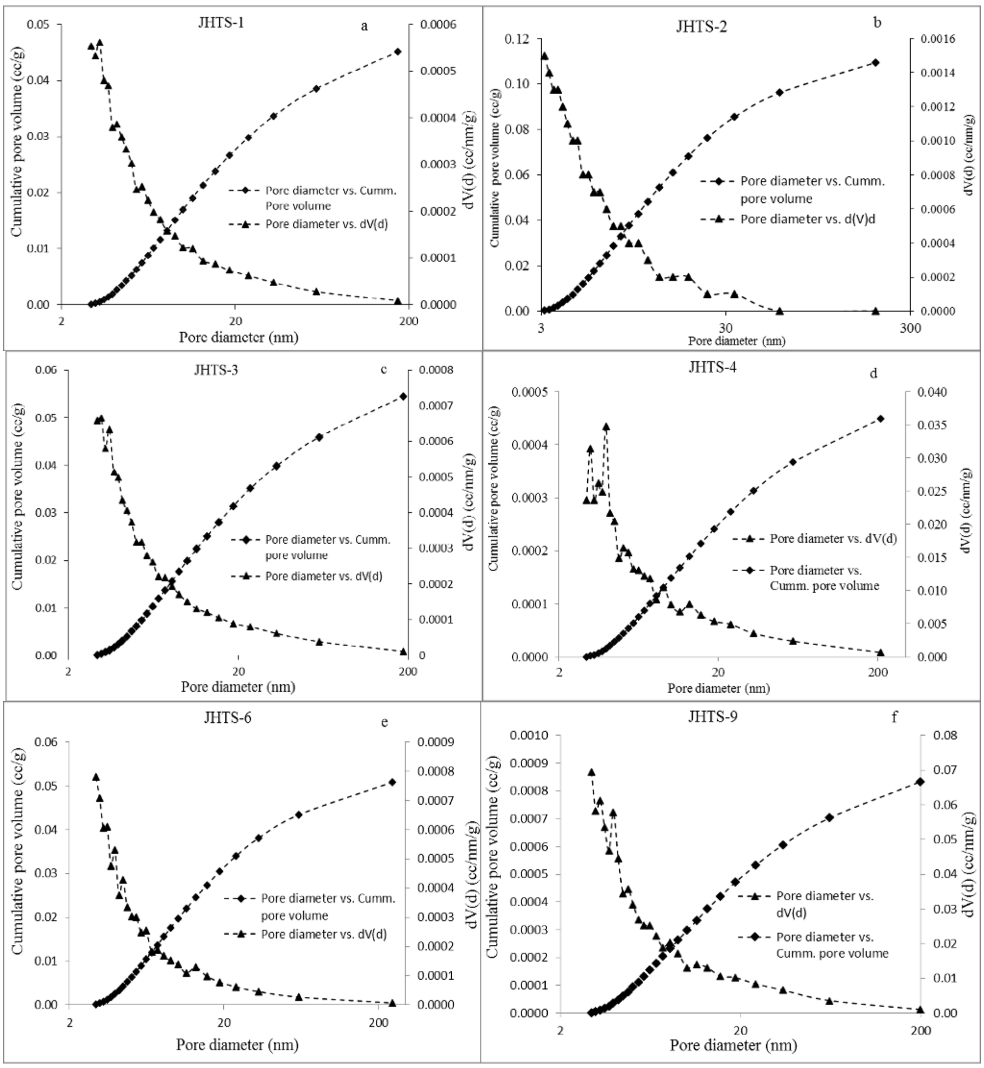

Figure 13. Estimation of pore size distribution in shale core samples by BJH method.

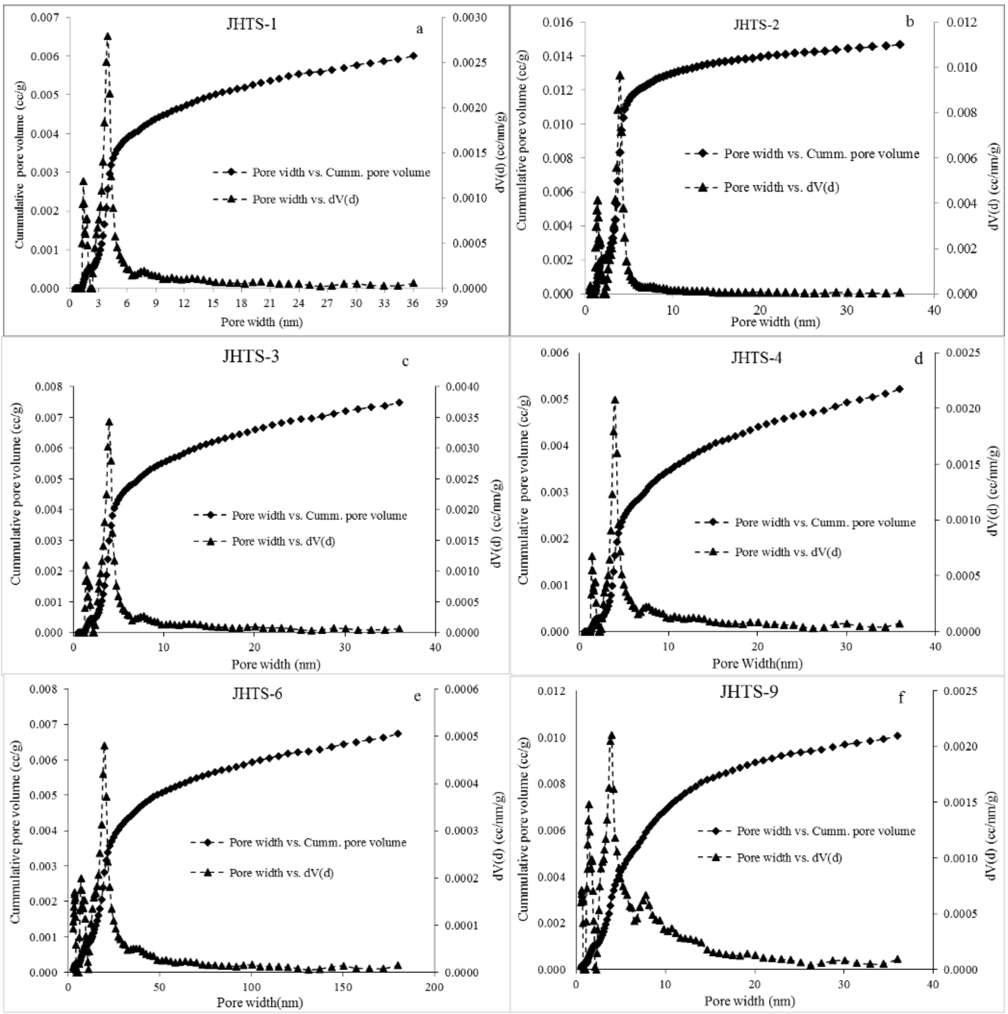

Figure 14. DFT plots for determination of surface area, pore size and pore volume of shale core samples.

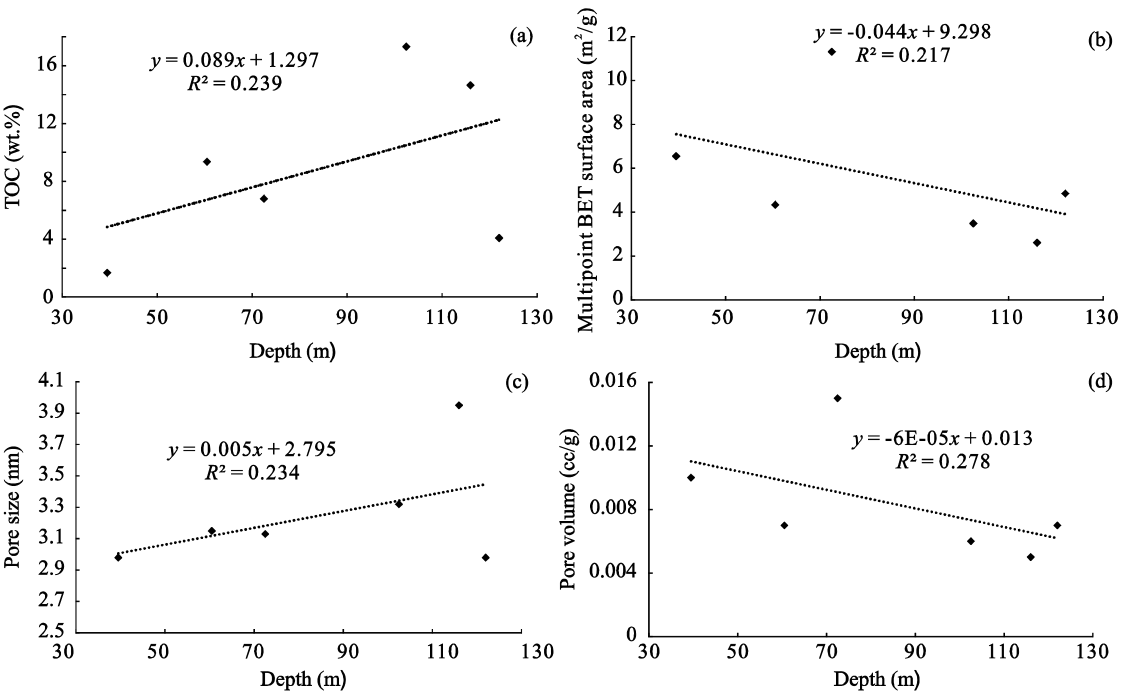

Figure 15. Plot of (a) depth vs. TOC, (b) depth vs. multipoint BET surface area, (c) depth vs. pore size, (d) depth vs. pore volume.

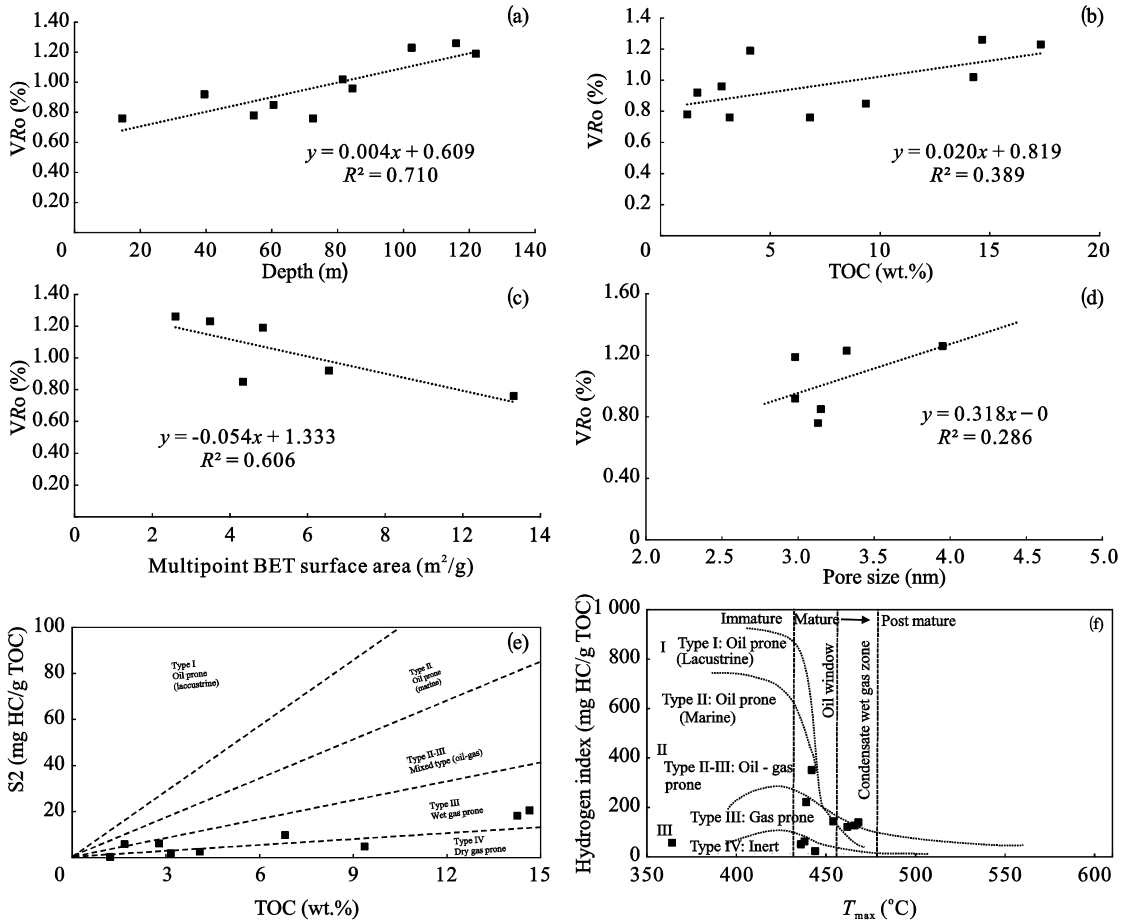

Figure 16. Plot of (a) depth vs. V*R*o, (b) TOC vs. V*R*o, (c) multipoint BET surface area vs. V*R*o, (d) pore size vs. V*R*o, (e) TOC vs. S2 and (f) T_{max} vs. HI.

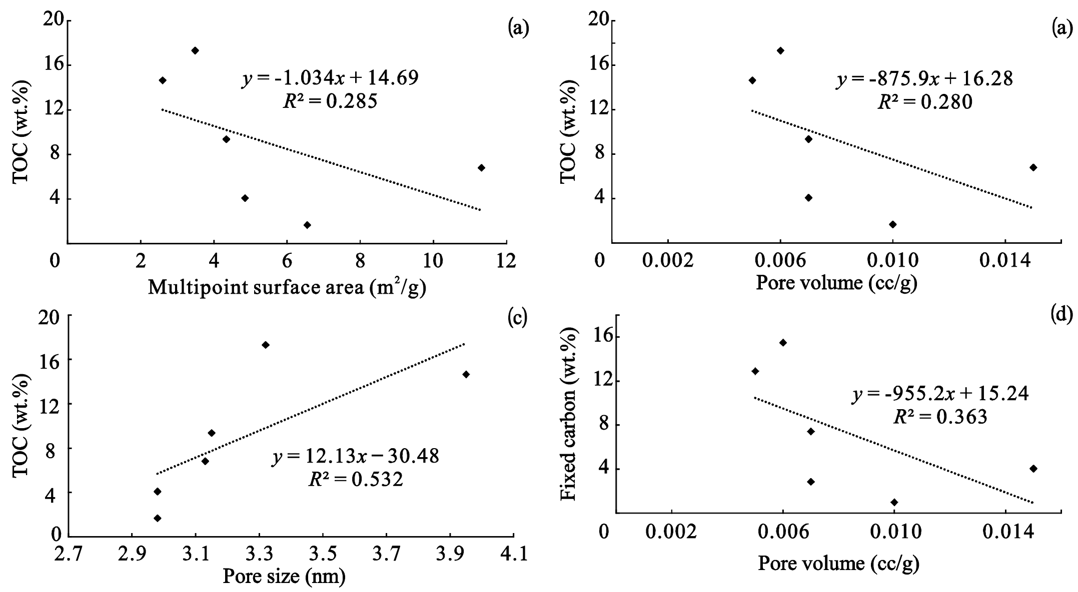

Figure 17. Plot of (a) multipoint BET surface area vs. TOC, (b) pore volume vs. TOC, (c) pore size vs. TOC, (d) pore volume vs. fixed carbon.

post depositional process and basin scale hydro-geologic circulation. The low pressure N_2 sorption isotherms are mostly Type II curve and H2 pattern represents the presence of dis-ordered and the distribution of pore size and shape is not well defined. However, the studied Barakar shales are significantly organic rich, thermally matured, having cylindrical, slit to bottle neck pores and encourages the further exploration and development of shales gas in Jharia Basin.

ACKNOWLEDGMENTS

The authors are indebted to Dr. P. K. Singh, CSIR-Central Institute of Miningand Fuel Research, Dhanbad for his constant encouragement to take up this research work and publication. We are also grateful to Ministry of Coal for funding support of the project entitled "Shale gas potentiality evaluation of Damodar Basin of India" (Coal S & T grant: CE(EoI)/30) under the research work has been carried out. The final publication is available at Springer via https://doi.org/10.1007/s12583-017-0779-8.

REFERENCES CITED

Aisharhan, A. S., Nairn, A. E. M., 2003. Sedimentary Basins and Petroleum Geology of the Middle East. Elsevier, The Netherlands. 944

Brooks, B. T., 1952. Evidence of Catalytic Action in Petroleum Formation. *Industrial & Engineering Chemistry*, 44(11): 2570–2577. doi:10.1021/ie50515a032

Brown, M. L., 2009. Analytical Trilinear Pressure Transient Model for Multiply Fractured Horizontal Wells in Tight Shale Reservoirs. [Dissertation]: Colorado School of Mines, Golden

Brunauer, S., Deming, L. S., Deming, W. E., et al., 1940. On a Theory of the van Der Waals Adsorption of Gases. *Journal of the American Chemical Society*, 62(7): 1723–1732. doi:10.1021/ja01864a025

Brunauer, S., Emmett, P. H., Teller, E., 1938. Adsorption of Gases in Multimolecular Layers. *Journal of the American Chemical Society*, 60(2): 309–319. doi:10.1021/ja01269a023

Bureau of Indian Standard (BIS), 1995. Methods of Test for Coal and Coke (Second Revision of IS: 1350). Part I, Proximate Analysis. Manak Bhawan, 9 Bahadur Shah Zafar Marg, New Delhi. 1–29

Casshyap, S. M., 1970. Sedimentary Cycles and Environment of Deposition of the Barakar Coal Measures of Lower Gondwana, India. *SEPM Journal of Sedimentary Research*, Vol. 40: 1302–1317. doi:10.1306/74d7218f-2b21-11d7-8648000102c1865d

Casshyap, S. M., Tewari, R. C., 1987. Depositional Model and Tectonic Evolution of Gondwana Basins. *The Palaeobotanist*, 36: 59–66

Chalmers, G. R. L., Bustin, R. M., 2007. The Organic Matter Distribution and Methane Capacity of the Lower Cretaceous Strata of Northeastern British Columbia, Canada. *International Journal of Coal Geology*, 70(1/2/3): 223–239. doi:10.1016/j.coal.2006.05.001

Chandra, D., 1992. Jharia Coalfield. Geological Society of India, Bangalore. 1–11

Chandra, S. K., 1990. Deposition of Bivalves in Indian Gondwana Coal Measures. *Indian Miner*., 44 (1): 31–44

Chandra, S. K., Betekhtina, O. A., 1990. Bivalves in Indian Gondwana Coal Measures. *Indian J. Geol*., 62(1): 18–26

Clarkson, C. R., Freeman, M., He, L., et al., 2012. Characterization of Tight Gas Reservoir Pore Structure Using USANS/SANS and Gas Adsorption Analysis. *Fuel*, 95: 371–385. doi:10.1016/j.fuel.2011.12.010

Claypool, G. E., 1998. Kerogen Conversion in Fractured Shale Petroleum Systems. AAPG Search and Discovery, Article #90937©1998, AAPG Annual Convention and Exhibition. Salt Lake City, Utah

Coal India Limited, 1993. Coal Atlas of India. CMPDI, Ranchi

Curtis, J. B., 2002. Fractured Shale-Gas Systems. *AAPG Bulletin*, 86: 1921–1938. doi:10.1306/61eeddbe-173e-11d7-8645000102c1865d

Curtis, M. E., Cardott, B. J., Sondergeld, C. H., et al., 2012. Development of Organic Porosity in the Woodford Shale with Increasing Thermal Maturity. *International Journal of Coal Geology*, 103: 26–31. doi:10.1016/j.coal.2012.08.004

de Boer, J. H., 1958. The Structure and Properties of Porous Materials. Butterworths, London. 68

Durand, B., Alpern, B., Pittion, L. J., et al., 1986. Reflectance of Vitrinite as a Control of Thermal History of Sediments. In: Burrus, J. ed., Thermal Modeling in Sedimentary Basins, Insitut Francais Petrole Research Conferences on Exploration, Carcan, France, June 3–7, 1985. Editions Technip, Paris. 441–473

EIA-Energy Information Administration, USA, 2011. World Shale Gas Resources: An Initial Assessment of 14 Regions Outside the United States, EIA Website. [2017-09-10] (2014-04). http://www.eia.gov/analysis/studies/worldshalegas [April 2011]

EIA-Energy Information Administration, USA, 2012. Annual Energy Review. [2017-09-10]. www.eia.doe.gov

Fu, H. J., Tang, D. Z., Xu, T., et al., 2017. Characteristics of Pore Structure and Fractal Dimension of Low-Rank Coal: A Case Study of Lower Jurassic Xishanyao Coal in the Southern Junggar Basin, NW China. *Fuel*, 193: 254–264. doi:10.13039/501100001809

Grim R. E., 1947. Relation of Clay Mineralogy to Origin and Recovery of Petroleum. *AAPG Bulletin*, 31: 1491–1499. doi:10.1306/3d933a1f-16b1-11d7-8645000102c1865d

Hakimi, M. H., Abdullah, W. H., Sia, S. G., et al., 2013. Organic Geochemical and Petrographic Characteristics of Tertiary Coals in the Northwest Sarawak, Malaysia: Implications for Palaeoenvironmental Conditions and Hydrocarbon Generation Potential. *Marine and Petroleum Geology*, 48: 31–46. doi:10.1016/j.marpetgeo.2013.07.009

Hardy, P., 2014. Chapter 1: Introduction and Overview: The Role of Shale Gas in Securing Our Energy Future in Fracking. Environmental Science and Technology, Royal Society of Chemistry, Thomas Graham House, Cambridge. 1–45. doi: 10.1039/9781782620556-00001

International Committee for Coal Petrology (ICCP), 1963. International Handbook of Coal Petrography: 2nd Ed. Centre National de la Recherche Scientifique, Paris

International Committee for Coal Petrology (ICCP), 1971. International Handbook of Coal Petrography (1st Supplement to 2nd Edition). International Committee for Coal and Organic Petrology, Unpagenated

International Committee for Coal Petrology (ICCP), 1973. International Handbook of Coal Petrography. Supplement to 2nd Ed. Centre National Recherche Scientifique, Paris

International Committee for Coal Petrology (ICCP), 1993. International Handbook of Coal Petrography. 2nd Ed., 3rd Supplement to 2nd Ed. University of New Castle, England

International Committee for Coal Petrology (ICCP), 1995. Vitrinite Classification. ICCP System 1994, Aachen. 1–24

International Committee for Coal Petrology (ICCP), 1998. The New Vitrinite Classification (ICCP System 1994). *Fuel*, 77: 349–358

International Energy Agency (IEA), 2007. World Energy Outlook—Global Energy Prospects: Impact of Developments in China & India. 1–674. http://www.worldenergyoutlook.org/media/weowebsite/2008-1994/weo_ 2007.pdf

IUPAC, 1997. Compendium of Chemical Terminology, 2nd ed. (the "Gold Book"). Compiled by A.D. McNaught and A. Wilkinson, Blackwell Scientific Publications, Oxford

Jacob, K., F. N. I., Ramaswamy, S. K., Rizvi, S. R. A., et al., 1958. Sedimentological Studies in Parts of Jharia and East Bokaro Coalfields. *Geological Survey of India*, 24A(6): 339–357

Jarvie, D. M., 2012. Shale Resource Systems for Oil and Gas: Part 1—Shale Gas Resource Systems. In: Breyer, J., ed., Shale Reservoirs—Giant Resources for the 21st Century. *American Association of Petroleum Geologists Memoir*, 97: 69–87

Jarvie, D. M., Hill, R. J., Ruble, T. E., et al., 2007. Unconventional Shale-Gas Systems: The Mississippian Barnett Shale of North-Central Texas as One Model for Thermogenic Shale-Gas Assessment. *AAPG Bulletin*, 91(4): 475–499. doi:10.1306/12190606068

Kuila, U., Prasad, M., 2013. Specific Surface Area and Pore-Size Distribution in Clays and Shales. *Geophysical Prospecting*, 61(2): 341–362. doi:10.1111/1365-2478.12028

Kuila, U., Prasad, M., Derkowski, A., et al., 2012. Compositional Controls on Mudrock Pore-Size Distribution: An Example from Nibrara Formation. SPE Annual Technical and Exhibition (October 8–10), San Antonio. http://dx.doi.org/10.2118/160141-MS

Labani, M. M., Rezaee, R., Saeedi, A., et al., 2013. Evaluation of Pore Size Spectrum of Gas Shale Reservoirs Using Low Pressure Nitrogen Adsorption, Gas Expansion and Mercury Porosimetry: A Case Study from the Perth and Canning Basins, Western Australia. *Journal of Petroleum Science and Engineering*, 112: 7–16. doi:10.1016/j.petrol.2013.11.022

Li, A., Ding, W. L., He, J. H., et al., 2016. Investigation of Pore Structure and Fractal Characteristics of Organic-Rich Shale Reservoirs: A Case Study of Lower Cambrian Qiongzhusi Formation in Malong Block of Eastern Yunnan Province, South China. *Marine and Petroleum Geology*, 70: 46–57. doi:10.13039/501100001809

Loucks, R. G., Reed, R. M., Ruppel, S. C., et al., 2009. Morphology, Genesis, and Distribution of Nanometer-Scale Pores in Siliceous Mudstones of the Mississippian Barnett Shale. *Journal of Sedimentary Research*, 79(12): 848–861. doi:10.2110/jsr.2009.092

Mani, D., Patil, D. J., Dayal, A. M., et al., 2015. Thermal Maturity, Source Rock Potential and Kinetics of Hydrocarbon Generation in Permian Shales from the Damodar Valley Basin, Eastern India. *Marine and Petroleum Geology*, 66: 1056–1072. doi:10.1016/j.marpetgeo.2015.08.019

Mastalerz, M., He, L. L., Melnichenko, Y. B., et al., 2012a. Porosity of Coal and Shale: Insights from Gas Adsorption and SANS/USANS Techniques. *Energy & Fuels*, 26(8): 5109–5120. doi:10.1021/ef300735t

Mastalerz, M., Schimmelmann, A., Lis, G. P., et al., 2012b. Influence of Maceral Composition on Geochemical Characteristics of Immature Shale Kerogen: Insight from Density Fraction Analysis. *International Journal of Coal Geology*, 103: 60–69. doi:10.1016/j.coal.2012.07.011

Mendhe, V. A., Mishra, S., Varma, A. K., et al., 2017a. Gas Reservoir Characteristics of the Lower Gondwana Shales in Raniganj Basin of Eastern India. *Journal of Petroleum Science and Engineering*, 149: 649–664. doi:10.1016/j.petrol.2016.11.008

Mendhe, V. A., Bannerjee, M., Varma, A. K., et al., 2017b. Fractal and Pore Dispositions of Coal Seams with Significance to Coalbed Methane Plays of East Bokaro, Jharkhand, India. *Journal of Natural Gas Science and Engineering*, 38: 412–433. doi:10.1016/j.jngse.2016.12.020

Mendhe, V. A., Mishra, S., Bannerjee, M., et al., 2017c. Evaluation of Thermal Maturity, Pore Structure and Behaviour of Gas Transport in Permian Shale Beds of Jharia Basin, Jharkhand. Proceedings of International Conference on NexGen Technologies for Mining and Fuel Industries (NxGnMiFu-2017), New Delhi. 1397–1408

Mendhe, V. A., Mishra, S., Kamble, A. D., et al., 2017d. Geological Controls and Flow Mechanism of Permian Gas Shale Reservoir of Raniganj Basin, West Bengal. *Journal of Geosciences Research*, 1: 161–172

Mendhe, V. A., Kamble, A. D., Bannerjee, M., et al., 2016. Evaluation of Shale Gas Reservoir in Barakar and Barren Measures Formations of North and South Karanpura Coalfields, Jharkhand. *Journal of the Geological Society of India*, 88(3): 305–316. doi:10.1007/s12594-016-0493-7

Mendhe, V. A., Mishra, S., Kamble, A. D., et al., 2015a. Shale Gas and Emerging Energy Resource: Prospects in India. *The Indian Mining & Engineering Journal*, 54(6): 21–31

Mendhe, V. A., Mishra, S., Varma, A. K., et al., 2015b. Coalbed Methane-Produced Water Quality and Its Management Options in Raniganj Basin, West Bengal, India. *Applied Water Science*, 7(3): 1359–1367. doi:10.1007/s13201-015-0326-7

Meyer, K., Klobes, P., 1999. Comparison between Different Presentations of Pore Size Distribution in Porous Materials. *Fresenius' Journal of Analytical Chemistry*, 363(2): 174–178. doi:10.1007/s002160051166

Mishra, S., Mani, D., Kavitha, S., et al., 2014. Organic Matter Characteristics and Gas Generation Potential of the Tertiary Shales from NW Kutch, India. *Journal of Petroleum Science and Engineering*, 124: 114–121. doi:10.1016/j.petrol.2014.10.019

Mishra, S., Mendhe, V. A., Kamble, A. D., et al., 2016. Prospects of Shale Gas Exploitation in Lower Gondwana of Raniganj Coalfield (West Bengal), India. *The Palaeobotanist*, 65: 31–46

Montgomery, S. L., Jarvie, D. M., Bowker, K. A., et al., 2005. Mississippian Barnett Shale, Fort Worth Basin, North-Central Texas: Gas-Shale Play with Multi-Trillion Cubic Foot Potential. *AAPG Bulletin*, 89(2): 155–175. doi:10.1306/09170404042

Moore, D. E., Morrow, C. A., Byerlee, J. D., 1982. Use of Swelling Clays to Reduce Permeability and Its Potential Application to Nuclear Waste Repository Sealing. *Geophysical Research Letters*, 9(9): 1009–1012. doi:10.1029/gl009i009p01009

Padhy, P. K., Das, S. K., 2013. Shale Oil and Gas Plays: Indian Sedimentary Basins. *Geohorizons*, 18: 20–25

Passey, Q. R., Bohacs, K. M., Esch, W. L., et al., 2010. From Oil-Prone Source Rock to Gas-Producing Shale Reservoir—Geologic and Petrophysical Characterization of Unconventional Shale-Gas Reservoirs. *Society Petroleum Engineers*, 2010: 131350

Person, M., Raffensperger, J. P., Ge, S. M., et al., 1996. Basin-Scale Hydrogeologic Modeling. *Reviews of Geophysics*, 34(1): 61–87. doi:10.1029/95rg03286

Pollastro, R. M., 2007. Total Petroleum System Assessment of Undiscovered Resources in the Giant Barnett Shale Continuous (Unconventional) Gas Accumulation, Fort Worth Basin, Texas. *AAPG Bulletin*, 91(4): 551–578. doi:10.1306/06200606007

Pophare, A. M., Mendhe, V. A., Varade, A., 2008. Evaluation of Coal Bed Methane Potential of Coal Seams of Sawang Colliery, Jharkhand, India. *Journal of Earth System Science*, 117(2): 121–132. doi:10.1007/s12040-008-0003-4

Quantachrome, 2014. Characterising Porous Materials and Powders AutosorbiQ and ASiQwin. *Gas Sorption System Operating Manual*, 2: 199–426

Roshan, H., Al-Yaseri, A. Z., Sarmadivaleh, M., et al., 2016. On Wettability of Shale Rocks. *Journal of Colloid and Interface Science*, 475: 104–111. doi:10.1016/j.jcis.2016.04.041

Ross, D. J. K., Marc, B. R., 2009. The Importance of Shale Composition and Pore Structure upon Gas Storage Potential of Shale Gas Reservoirs. *Marine and Petroleum Geology*, 26(6): 916–927. doi:10.1016/j.marpetgeo.2008.06.004

Rouquerol, F., Rouquerol, J., Sing, K. S. W., 1999. Adsorption by Powders and Porous Solids. Academic Press, London

Ruppel, S. C., Loucks, R. G., Gale, J. F. W., 2008. Barnett, Woodford, and Related Mudrock Successions in Texas Cores and Outcrops. A Core Workshop Prepared for the 2008 AAPG/SEPM, Annual Convention, Austin. 82

Schlumberger, M., 2012. China's Anton Oilfield Eyes More Opportunities with Schlumberger Partnership. Platts Commodity News, 12 July 2012, via Factiva, © 2012 Platts

Schmoker, J. W., 1995. Method for Assessing Continuous-Type (Unconventional) Hydrocarbon Accumulations. In: Gautier, D. L., Dolton, G. L., Takahashi, K. I., et al., eds., National Assessment of United States Oil and Gas Resources—Results, Methodology, and Supporting Data. U. S. Geological Survey Digital Data Series, DDS-30

Sen, S., Das, N., Maiti, D., 2016. Facies Analysis and Depositional Model of Late Permian Raniganj Formation: Study from Raniganj Coal Bed Methane Block. *Journal of the Geological Society of India*, 88(4): 503–516. doi:10.1007/s12594-016-0513-7

Sengupta, N., 1980. A Revision of the Geology of the JCF with Particular Reference to Distribution of Coal Seam: [Dissertation]. ISM, Dhanbad, India

Shiver, R., Nelsen, K., Li, E., et al., 2015. Unconventional Shale Reservoir's Property Estimation through Modeling, Case Studies of Australian Shale. *Energy and Power Engineering*, 7(3): 71–80. doi:10.4236/epe.2015.73007

Sing, K. S. W., Everett, D. H., Haul, R. A. W., et al., 1985. Reporting Physisorption Data for Gas/Solid Systems with Special Reference to the Determination of Surface Area and Porosity. *Pure Applied Chemistry*, 57: 603–619

Sing, K., 2001. The Use of Nitrogen Adsorption for the Characterisation of Porous Materials. *Colloids and Surfaces A*: *Physicochemical and Engineering Aspects*, 187–188: 3–9. doi:10.1016/s0927-7757(01)00612-4

Singh, H., 2016. A Critical Review of Water Uptake by Shales. *Journal of Natural Gas Science and Engineering*, 34: 751–766. doi:10.13039/100000015

Taylor, G. H., Teichmuller, M., Davis, A., et al., 1998. Organic Petrology. Gebruder Borntranger, Berlin

Tewari, R. C., Casshyap, S. M., 1982. Paleoflow Analysis of Late Paleozoic Gondwana Deposits of Giridih and Adjoining Basins and Paleogeographic Implications. *Journal of Geological Society of India*, 23(2): 67–79

Tewari, R. C., Casshyap, S. M., 1983. Cyclicity in Early Permian Fluviatile Gondwana Coal Measures: An Example from Giridih and Saharjuri Basins, Bihar, India. *Sedimentary Geology*, 35(4): 297–312. doi:10.1016/0037-0738(83)90063-5

Tissot, B. P., Welte, D. H., 1978. Petroleum Formation and Occurrence: A New Approach to Oil and Gas Exploration. Springer-Verlag, New York. 720

USGS, 1986. USGS Research on Energy Resources-Program and Abstracts. V. E. Mckelvey Forum on Mineral and Energy Resources, U.S. Geological Circular, 974

Uysal, I. T., Glikson, M., Golding, S. D., et al., 2004. Hydrothermal Control on Organic Matter Alteration and Illite Precipitation, Mt Isa Basin, Australia. *Geofluids*, 4(2): 131–142. doi:10.1111/j.1468-8115.2004.00077.x

Varma, A. K., Hazra, B., Mendhe, V. A., et al., 2015. Assessment of Organic Richness and Hydrocarbon Generation Potential of Raniganj Basin Shales, West Bengal, India. *Marine and Petroleum Geology*, 59: 480–490. doi:10.1016/j.marpetgeo.2014.10.003

Varma, A. K., Hazra, B., Samad, S. K., et al., 2014. Methane Sorption Dynamics and Hydrocarbon Generation of Shale Samples from West Bokaro and Raniganj Basins, India. *Journal of Natural Gas Science and Engineering*, 21: 1138–1147. doi:10.1016/j.jngse.2014.11.011

Wang, L., Torres, A., Xiang, L., et al., 2015. A Technical Review on Shale Gas Production and Unconventional Reservoirs Modeling. *Natural Resources*, 6(3): 141–151. doi:10.4236/nr.2015.63013

Wang, M., Yang, J. X., Wang, Z. W., et al., 2015. Nanometer-Scale Pore Characteristics of Lacustrine Shale, Songliao Basin, NE China. *PLOS ONE*, 10(8): e0135252. doi:10.1371/journal.pone.0135252

Wei, L., Wang, Y. Z., Mastalerz, M., 2016. Comparative Optical Properties of Macerals and Statistical Evaluation of Mis-Identification of Vitrinite and Solid Bitumen from Early Mature Middle Devonian—Lower Mississippian New Albany Shale: Implications for Thermal Maturity Assessment. *International Journal of Coal Geology*, 168: 222–236. doi:10.13039/100000015

Wintsch, R. P., Christoffersen, R., Kronenberg, A. K., 1995. Fluid-Rock Reaction Weakening of Fault Zones. *Journal of Geophysical Research*: *Solid Earth*, 100(B7): 13021–13032. doi:10.1029/94jb02622

Zhao, P. Q., Ma, H. L., Rasouli, V., et al., 2017. An Improved Model for Estimating the TOC in Shale Formations. *Marine and Petroleum Geology*, 83: 174–183. doi:10.13039/501100004701